Journal of Intelligent Manufacturing (2024) 35:1407–1437
https://doi.org/10.1007/s10845-023-02119-y

Process monitoring and machine learning for defect detection in laser-based metal additive manufacturing

T. Herzog[1,2] · M. Brandt[1] · A. Trinchi[2] · A. Sola[2] · A. Molotnikov[1]

Received: 4 May 2022 / Accepted: 17 March 2023 / Published online: 13 April 2023
© The Author(s) 2023

Abstract

Over the past several decades, metal Additive Manufacturing (AM) has transitioned from a rapid prototyping method to a viable manufacturing tool. AM technologies can produce parts on-demand, repair damaged components, and provide an increased freedom of design not previously attainable by traditional manufacturing techniques. The increasing maturation of metal AM is attracting high-value industries to directly produce components for use in aerospace, automotive, biomedical, and energy fields. Two leading processes for metal part production are Powder Bed Fusion with laser beam (PBF-LB/M) and Directed Energy Deposition with laser beam (DED-LB/M). Despite the many advances made with these technologies, the highly dynamic nature of the process frequently results in the formation of defects. These technologies are also notoriously difficult to control, and the existing machines do not offer closed loop control. In the present work, the application of various Machine Learning (ML) approaches and in-situ monitoring technologies for the purpose of defect detection are reviewed. The potential of these methods for enabling process control implementation is discussed. We provide a critical review of trends in the usage of data structures and ML algorithms and compare the capabilities of different sensing technologies and their application to monitoring tasks in laser metal AM. The future direction of this field is then discussed, and recommendations for further research are provided.

Graphical abstract

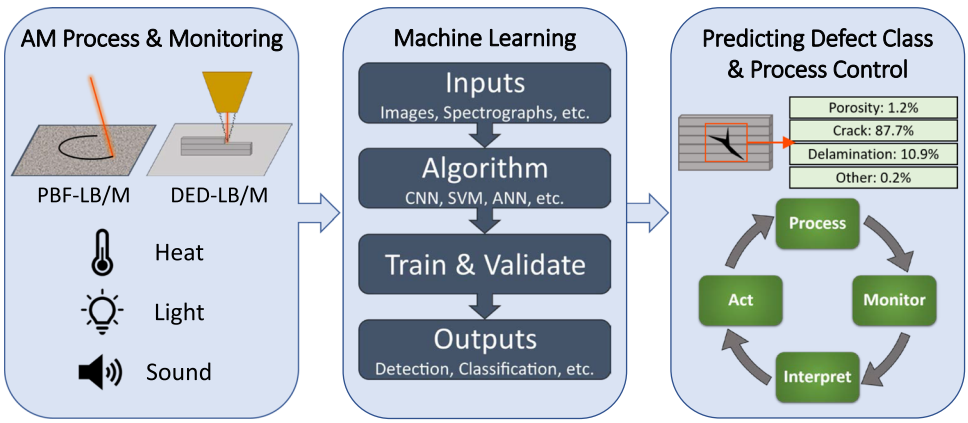

Keywords Additive manufacturing · In-situ monitoring · Process control · Machine learning · Laser powder bed fusion · Directed energy deposition

✉ T. Herzog
s3826323@student.rmit.edu.au

✉ A. Molotnikov
andrey.molotnikov@rmit.edu.au

[1] Centre for Additive Manufacturing, School of Engineering, RMIT University, Melbourne, VIC 3000, Australia

[2] CSIRO Manufacturing Business Unit, Clayton, VIC 3168, Australia

Introduction

The additive manufacturing (AM) industry has proliferated over the past few decades, from a modest beginning in the late 1980s with the advent of stereolithography (Wohlers & Gornet, 2014) to a global industry predicted to exceed US$34 billion by 2024 (Jayaram et al., 2020). In particular, metal AM has begun to infiltrate many high-value industries with applications in aerospace, automotive, medical and nuclear energy (Brandt, 2017; Wohlers & Gornet, 2014), to name a few. Metal AM is capable of producing custom, complex, near net-shaped parts directly, with minimal waste, and has enabled many advancements within industry. Parts with reduced mass have improved the fuel efficiency of aircraft and automotive vehicles (Cooper et al., 2015), while readily customisable designs have increased the quality of life for patients with medical implants and prosthetic limbs (Shaunak et al., 2017). Recent AM-driven developments, such as functionally graded materials (FGMs), parts with intentionally varied structure or composition, and multi-material parts, both difficult to produce by traditional methods, are very promising in their potential for providing tailored mechanical responses within a single component (Zhang et al., 2020; Zhiyuan Xu et al., 2019). Of the various AM technologies for manufacturing metal parts, Directed Energy Deposition (DED) and Powder Bed Fusion (PBF) are the most prolific. Several excellent books were published in 2021 and provide an extensive explanation of these technologies; see Toyserkani et al. (2021) and Yadroitsev et al. (2021). Here, a short description of both processes is provided below.

In the present work standard ISO/ASTM 52900:2021 is adhered to for naming of AM processes, following the form 'process category – process feature/material class/specific material(s)', such that DED using a laser beam (LB) of the metal (M) alloy, Ti6Al4V, is referred to as DED-LB/M/Ti6Al4V.

Metal DED processes bear a resemblance to some welding techniques in that an energy source, typically a laser (DED-LB/M), electron beam (DED-EB/M) or electrical/plasma arc (DED-Arc/M) (Oliveira et al., 2020), is used to melt a feedstock onto a surface depositing a weld bead. This weld bead can be deposited over a surface to provide a metallurgically bonded cladding, layered upon damaged surfaces to repair them, or deposited along contours and internal structures to build up an entire component. Feedstock materials can be in either wire or powder form, with powder being blown into the melt pool by an inert carrier gas and wire mechanically fed into the melt pool. Typically, wire feedstocks allow for faster volumetric build rates, while powder-fed systems can achieve tighter dimensional tolerances and allow for the creation of FGMs by powder mixing (Loh et al., 2018). The three-fold application of cladding, repair, and construction highlights the usefulness of DED to industry in its current state. However, this technology does have some drawbacks, such as limited overhang angles, poor dimensional tolerances, potentially high residual stresses, and limited ability to produce complex shapes, which currently limit its broader applications. Other common terminologies include Laser Metal Deposition (LMD), Laser Engineered Net Shaping (LENS™) or Directed Laser Deposition (DLD).

Similarly, metal PBF processes utilise an energy source, a laser (PBF-LB/M) or electron beam (PBF-EB/M), to selectively fuse metallic powders into a solid component. The energetic beam is scanned across the surface of the powder bed, consolidating the powder. Laser systems rely on high-speed XY galvanometers to move the beam, while electron beams are directed by magnetic coils, allowing for inertia-free motion and higher scan speeds. Once the entire cross-section of a layer has been scanned, the build platform is lowered by the desired layer thickness, a fresh layer of powder is spread across the surface, and the process repeated (Brandt, 2017). After completion, the part can be removed, and the loose powder recycled for future print jobs. PBF-LB/M is typically preferred to DED-LB/M for the manufacture of components requiring high dimensional accuracies, as it generally utilises smaller layer thicknesses and spot sizes (DebRoy et al., 2020). Additionally, the surrounding powder bed provides some support for overhangs, resulting in better control over the part geometry, producing finer features, and aiding in heat dissipation. Although unsupported overhanging structures can develop substantial surface roughness, this can be mitigated with optimised process parameters (DePond et al., 2018).

Despite the opportunities that metal AM presents, there are still several barriers to its widespread industrial adoption. Both PBF-LB/M and DED-LB/M require highly trained technical staff to initiate, monitor and remove components once built, contrary to conventional manufacturing, where automation has continually increased over the past few decades. Additionally, components produced by AM are often plagued by the occurrence of process-induced defects, such as pores, cracks, and distortion due to residual stresses, impairing both part quality and consistency. Process-induced defects within a part can reduce the mechanical and fatigue properties (du Plessis et al., 2020; Elambasseril et al., 2019; Malefane et al., 2018), causing it to fail below designed operational limits. Industrial manufacturing frequently employs rigorous quality standards to ensure conformance and performance of components. As AM processes generally produce parts individually or in small batches, it becomes expensive and difficult to provide the same statistical quality assurance that can be achieved with traditional manufacturing

processes. Therefore, it has frequently been identified in the literature (Bourell et al., 2009; Scime & Beuth, 2018a) that quality control of AM processes remains the outstanding issue hindering further adoption of AM by high-value industries.

Process-induced defects

The formation of process-induced defects presents a significant challenge to industrial uptake of laser AM technologies. The presence of defects can be highly inhomogeneous (Carlton et al., 2016), leading to unpredictable variation in physical properties between parts or within the same part. Post-processing strategies can be an effective method for reducing some critical defects in parts, contributing to a significant improvement in the reliability of AM components. Machining and surface polishing notably prolong fatigue life (Brandão et al., 2017) but are only applicable to parts with accessible surfaces; heat treatment can relieve internal stresses and improve ductility (Gibson et al., 2014; Girelli et al., 2019); and hot isostatic pressing (HIP) can close cracks and pores in many instances (du Plessis & Macdonald, 2020). However, post-processing is not always sufficient to rectify all critical defects and increases manufacturing time and cost. Therefore, it is desirable to minimise the formation of defects during the production of the part itself.

Laser metal AM processes consist of highly dynamic interactions between energy source, feedstock, substrate, and environment to produce a final part, allowing for various defects to form. Some of the common process-induced defects in laser metal AM are summarised in Table 1. For detailed explanations of the formation mechanisms, the reader is referred to the following works: Bayat et al. (2019), Chen and Yan (2020), du Plessis et al. (2020), Elambasseril et al. (2019), Khairallah et al. (2016), Oliveira et al. (2020), Sammons et al. (2019), Stockman et al. (2019), Sun et al. (2017), Thompson et al. (2015), and Zhao et al. (2017).

Porosity is a common defect in all AM processes, particularly those requiring powders for feedstock. Keyhole-induced pores, most common in PBF processes, form when excessive energy is deposited into the surface, causing the melt pool to penetrate deep into the previous layers. Recoil pressure and Marangoni flow generate a depression and cavity down into the centre of the melt pool (Bayat et al., 2019) to form the keyhole. Fluid instabilities then cause the top of the cavity to close over, producing a void at the bottom which moves back and upwards through the melt pool, becoming spheroidal in shape to minimise surface energy. These voids may escape the melt pool while it is still liquid; otherwise, they become entrapped by the solidification front as pores (Bayat et al., 2019). Lack of fusion pores are generally formed by insufficient energy density being delivered to the surface, which may result in incomplete melting of powders or tracks not properly bonding to each other and can occur in both PBF-LB/M and DED-LB/M processes. These pores are irregular in shape and can act as stress concentrators (du Plessis et al., 2020), impacting mechanical and fatigue performance. Other gas-filled pores can form when powders entrain gasses with them into the melt pool or contain pores from the powder manufacturing process. These may be consumed by other pores, escape, dissolve or become trapped in the solidified material (Chen et al., 2020).

Table 1 Summary of common process-induced defects, their causes, and potential effects on part quality in laser metal AM

Common defect types	Common causes	Potential effects
Keyhole pores	Excessive input energy density	Reduction in mechanical properties Reduction in fatigue properties
Lack of fusion (LOF) pores	Insufficient input energy density	Reduction in mechanical properties Reduction in fatigue properties
Gas pores	Gas entrapped in feedstock Gas entrained into the melt pool	Reduction in fatigue properties
Cracking and delamination	Residual stresses exceeding the local ultimate tensile strength Insufficient bonding between layers	Part failure
Deformation	Residual stresses exceeding the local yield stress	Conformance failure
Alloy compositional variance	Improper powder deposition Differing chemical mobility Preferential evaporation Gas incorporation/adsorption	Inhomogeneous mechanical properties
Balling	Low/High input energy density Surface oxidation	Part/Conformance failure Formation of other defects
Rippling	Instabilities of layer-to-layer deposition	Part failure/Production failure
Spatter/Particle ejection	Overheated melt pool Recoil pressure and melt plume	Formation of other defects

The extremely high thermal gradients and cooling rates generated by the additive process can lead to uneven contraction of the component, giving rise to residual stresses within the part. These residual stresses distort the part from its intended geometry and can be significant enough to render the component unusable. Alternatively, these stresses can cause the printed part to fracture, either between successive layers as delamination or through multiple layers as cracking (de Oliveira et al., 2006; Oliveira et al., 2020). These stresses are computationally expensive to model or predict (Wang et al., 2021) and contribute significantly to process inconsistency.

Current approaches for the detection of process-induced defects

Current practices for the detection of process-induced defects rely on post-production inspection. This is known as ex-situ or post-mortem monitoring and can be carried out by destructive and non-destructive testing methods. While destructive testing can provide helpful information for studying the effect of processing parameters on the formation of microstructure and mechanical properties, non-destructive testing methods, such as X-ray Computed Tomography (XCT), can allow for internal defects to be mapped without compromising the component (du Plessis et al., 2020). Despite the clear benefits of non-destructive testing, these methods are expensive and time-consuming (Montazeri et al., 2019). For example, to obtain high spatial resolution in XCT creates very large datasets, and the scanned volume is typically kept small. Stitching of smaller volumes can be achieved, but this also increases the volume of data and acquisition time. Large sample volumes can also be scanned, however, this comes at the cost of spatial resolution (Withers et al., 2021). Both methods provide value for part certification and defect research, but only provide information on the final product and thus are limited in their ability to monitor the actual formation of defects.

Recently, there has been a rapid increase in research aimed at understanding and reducing the formation of process-induced defects in metal AM. Machine Learning (ML) algorithms are beginning to be employed for defect detection and quality prediction in metal AM. These algorithms can effectively interrogate the large amounts of data generated by in-situ monitoring of the additive process and help to elucidate the relationships between process specific input parameters and final part quality.

Several reviews have begun to address different aspects of this body of literature including the development of sensor technologies for various DED systems (Tang et al. (2020)), and image-based (Wu et al., 2021) and generic (Grasso et al., 2021) monitoring methods for PBF. Other examples include reviews of monitoring and process control in PBF-LB/M by McCann et al. (2021) and Mahmoud et al. (2021), as well as the work by Fu et al. (2022), which provides an analysis of ML algorithms that have been used for defect detection in both DED-LB/M and PBF-LB/M.

This present work provides a holistic review on the combination of dominant laser AM processes (DED-LB/M and PBF-LB/M), relevant monitoring technologies and the defect types they can detect, with the application of ML approaches for various purposes. Specifically, the differences in sensor capabilities, implementation, and data generation will be critically discussed for both DED-LB/M and PBF-LB/M. This work will highlight how various studies are using these data streams to foster automatic defect detection, identify trends in process monitoring research, and how these are advancing progress towards effective closed-loop process control where process parameters are modulated to maintain ideal build conditions based on interpreted signals.

The scope of this work will be confined to investigations of metal AM where the applied energy is in the form of a laser beam. This ensures more direct comparison between research works as the underlying physical interactions are closely related within this classification. Additionally, laser AM provides for various monitoring opportunities, such as utilisation of the optical train, and observing laser reflections, as well as challenges, such as plume interference, high temperatures and high process speeds. Therefore, only in-situ sensor technologies, automated defect detection methods, and process control methods applicable to these technologies will be discussed in detail.

This work will be organised as follows. "Machine learning" section of this work will provide an overview of the most common ML algorithms relevant to this field and the data structures that are most relevant to them. "In-situ monitoring of additive manufacturing" section will review the technologies currently applied to in-situ monitoring of AM processes, grouped by the type of signal to be monitored. This will provide a discussion of sensor implementation, signal resolution and the generated data structures. "Analysis of in-situ data" section will assess the techniques available for analysing the data for automatic detection and prediction of defects, contrasting ML approaches with other analysis techniques. The potential future of monitoring and detection for closed-loop process control in laser AM will be discussed in "Discussion and future directions" section. A list of all abbreviations used in the text can be found in "Appendix 1."

Machine learning

ML is a branch of artificial intelligence (AI) which uses algorithms that progressively adjust a program's response to input data, achieving remarkable success in many different fields as computing power and program design have

advanced. In particular, Deep Learning (DL) has seen enormous progress in the last two decades for many classification and recognition tasks, outperforming all other computer-based methods (Lecun et al., 2015). DL approaches have already been applied to active industrial systems to help control the processing conditions (Wu et al., 2020), and recent research has been conducted to extend their use to inspection (Baumgartl et al., 2020; Li et al., 2020; Shevchik et al., 2018; Zhang et al., 2019a) and control (Kwon et al., 2020) for metal AM.

ML approaches can be grouped into four general categories: supervised, unsupervised, semi-supervised, and reinforcement learning (RL), based on the input–output structure of the training data. A brief description of each learning format can be found in "Appendix 2."

ML approaches can accommodate various data types, from visible images to acoustic signals and extracted feature vectors. As such, the multiple in-situ monitoring methods described in "In-situ monitoring of additive manufacturing" section lend themselves to different ML approaches. For example, visual (Yuan et al., 2018) and thermal (Baumgartl et al., 2020) imaging produces spatially resolved images that can be used directly in Convolutional Neural Networks (CNNs) or processed to extract metrics used by other algorithms (Liu et al., 2019), such as the Support Vector Machine (SVM). In "Machine learning to predict anomalies" section, the prevalence of various ML approaches for defect detection is discussed in greater detail. However, some of the more commonly used algorithms will be briefly addressed here.

Artificial neural networks

Artificial Neural Networks (ANNs), sometimes referred to as simply Neural Networks (NNs), are a class of ML algorithm that are constructed from a series of interconnected nodes, or neurons, in multiple layers with the basic structure of an input layer, one or more hidden layers and an output layer. Each neuron accepts input signals from one or more preceding neurons, performs a mathematical operation on them, and outputs a numerical signal to the neurons in the following layer (Meng et al., 2020). The definition of the mathematical operation will depend on the network architecture and purpose, but the simplest versions multiply the output of each neuron in the preceding layer by a weight value, and then the resultant weighted inputs are summed together. If the summation is greater than some threshold value, the neuron is 'activated' and will then pass on a signal to the next layer of neurons (Soni et al., 2021). The simplest implementation of this is as a binary signal, '1' if the neuron is activated, and '0' if not. More commonly, non-linear so-called 'activation functions' are used instead, such as the hyperbolic tangent function, tanh, which provides a bounded output between -1 and 1 (Gardner & Dorling, 1998; Soni et al., 2021).

The weights are updated during the training of an ANN, usually via a process known as back propagation, to minimise the difference between a prediction and target (Gardner & Dorling, 1998). ANNs span a large family of different algorithms, including CNNs (Soni et al., 2021). However, the present work considers the most commonly used variants independently due to their prevalence and specialised architectures. As the structure of ANNs are highly flexible and customised based on the desired function, they can accept input from a wide variety of sensor type, as long as the input data can be vectorized. For example, features from thermal images (), spectral intensity ratios (Montazeri et al., 2020) or a concatenated input from various sensors (Petrich et al., 2021) can be used for training ANNs.

Convolutional neural networks

CNNs are well renowned for its ability to learn key features from image-based data, forming the basis for autonomous cars and robotic vision (Lecun et al., 2015). This can be extended from purely image data from thermal or visible light cameras, to any array-based data structure with spatial relationships between points, such as the spectral graphs utilised by Shevchik et al. (2018) for classifying porosity levels in PBF-LB/M/CL 20ES. The CNN structure includes smaller filters that convolve over the data array and learn various features (lines, curves, etc.), which are then output as feature maps indicating where these features occur. Convolutions are then carried out on these feature maps, identifying more complex features. Pooling operations are then also applied between convolutions to concentrate similar features into a smaller space, whilst preserving their arrangement and making the network invariant to small shifts in relative feature positions. Through a combination of convolution and pooling operations, a CNN learns to recognise images and array data in a similar fashion to how a human does (Lecun et al., 2015).

Support vector machines

SVMs have frequently been used to classify data from in-situ monitoring. An SVM generally accepts features or data points that can be extracted from the sensor and learns how to separate the data of different classes with an optimal hyperplane. If two-dimensional data is non-separable, then the SVM will cast the data into three or higher dimensions, constructing a hyperplane that will separate the data, resulting in an (n−1)-dimensional plane to separate data in n-dimensions (Campbell & Ying, 2011). This approach can be used wherever it is possible to extract features from data, such as melt pool geometry from image analysis (Liu et al., 2019), processing parameters or spectrometer ratios (Montazeri et al., 2019). These features may be predetermined or calculated

through Principal Component Analysis (PCA), although it was shown by Montazeri et al. (2019) that features extracted by PCA may prove more efficient at capturing relevant data than pre-determined features.

K-Nearest Neighbours

K-Nearest Neighbour (KNN) algorithms operate on the assumption that data points sharing characteristics with other points are close to them in a parameter space. The distance between points in this space is a function of their similarity, with similar points grouping together (Khanzadeh et al., 2018). For example, if laser power and scan speed were the two parameters being used for mapping, and the track density was the characteristic being measured, it could be assumed that two data points with similar speed and power would have similar track density. Hence, when a new data point is being classified, the algorithm will look at the labels of the closest data points to determine the most likely label for this new data point. The value of 'k' is the number of nearest neighbours considered, and typically a majority voting approach is used, such that the most common label in that set is the label assigned to the new datum (Chen et al., 2021a). The distance itself can be calculated in various ways, depending on the specific problem being solved. This process extends into higher-dimensional spaces too, such that, given a coordinate vector, z, in a vector space with N observations, 'k' nearest neighbours are consulted to determine the most likely label for the query (Khanzadeh et al., 2018). This allows for a similar variety of sensors to be applicable to this algorithm, as for ANNs, with spectral data again being used by Montazeri et al. (2020) and features extracted from thermal imaging used by Khanzadeh et al. (2018).

Tree algorithms

Decision Trees (DTs) form the basis for the group of tree-based ML algorithms. A DT is a classifier network that utilises a series of nodes and branches to sort input data. Typically, each node of the tree will sort an input vector based on one or more characteristics, most simply by applying a threshold to one attribute of the vector, such as the features extracted from thermal imaging by Khanzadeh et al. (2018). These thresholds are updated during the training process to obtain the best classification of the training data. It is important to note that the input data can be categorical or numerical, unlike NNs, which require numeric data only, preserving more information from the data source (Günlük et al., 2021). Random Forest (RF) algorithms build an ensemble of DTs using subsets of training data and then aggregate the results to form a classifier that is more robust than a single DT. This approach was used to detect porosity in DED-LB/M/Ti6Al4V builds via image classification by Behnke et al. (2021). The k-D tree is an extension of a DT into 'k' dimensions, where each node separates the data in k-dimensions (Bentley, 1975) and has been used for classifying pyrometry data to detect porosity in PBF-LB/M/SS316L by Mitchell et al. (2020).

Deep Belief Networks

The Deep Belief Network (DBN) is a DL algorithm constructed from two or more smaller units, known as Restricted Boltzmann Machines (RBMs). An RBM is similar in structure to an ANN in that it has one input (or visible) layer and one hidden layer; however, there is no output layer for each of them in the same way as there is for an ANN. When stacked into a DBN, the hidden layer from one RBM forms the visible layer for the subsequent RBM (Le Roux & Bengio, 2008). An output layer is applied to the end of the stack only, such as the 'softmax' layer used in Ye et al. (2018a) where extracted plume and spatter data from thermal images were used to classify PBF-LB/M/SS304L melt state. Training is carried out in two steps, where the input into the first RBM is used for unsupervised training of the RBM to learn to represent the features of the input. This is then carried forward to the next RBM, which allows the network to learn higher-level features (Ye et al., 2018a). The network weights are then fine-tuned through a supervised learning process as described for the cases of acoustic monitoring (Ye et al., 2018a) and melt pool imaging with extracted features (Li et al., 2022).

In-situ monitoring of additive manufacturing

This section will provide an overview of some of the common technologies currently applied for in-situ monitoring within laser metal AM and explore some representative examples of their implementation. This is motivated by the necessity of understanding how data can be captured in-situ for ML approaches to defect detection. The underlying thermal interactions between the laser and the feedstock in both PBF-LB/M and DED-LB/M are relatively similar in that they both rely on the laser to provide heat to the powder (or wire), generally melting it completely to form a melt pool. The melt pool then solidifies on top of previous layers or substrate to form the desired shape. There are, obviously, significant differences in the setup of these processes, which necessitate different approaches to monitoring, but the targets may often be similar, and most sensors can be adapted to either process. For example, imaging of the melt pool can be achieved coaxially for both PBF-LB/M and DED-LB/M if there are mounting ports coupled to the optical train. If not available, then off-axis monitoring is typically the only recourse. The considerations for coaxial and off-axial

monitoring are discussed further in "Coaxial mounting" and "Off-axis mounting" sections.

One key difference between the image-based monitoring and defect detection of DED-LB/M and PBF-LB/M processes is the accessibility of the surfaces. During PBF-LB/M, only the top layer is visible at any one time, which limits the information accessible by the camera. Thermal imaging and digital image correlation (DIC) can be used to identify some defects (Baumgartl et al., 2020), such as pores and distortion, but few defects below the powder bed surface will be identifiable if they form after new layer additions. By contrast, DED-LB/M parts are built free-standing, providing line-of-sight access to lower areas of the build. This can allow for effects of heat accumulation and thermal cycling to be observed on lower layers that would not be detectible if the part was submerged in a powder bed, as modelled in Biegler et al. (2020). Other than this, most other differences in defect detectability rely on the application of sensors and the monitoring target of individual studies. However, the typically higher scan rate and smaller spot size of PBF-LB/M make an increased temporal and spatial resolution more important than when trying to measure the same metrics in DED-LB/M.

The remainder of this section is separated by the five primary signal categories (plus other, less common categories) relevant to AM monitoring, with Fig. 1 below providing an overview of these categories. Each section will summarise how these monitoring technologies are implemented and provide examples where data from these were used for automated defect detection by ML. The range of reported capabilities of these sensors is summarised in Table 2 for ease of comparison.

Visible light

Visible light monitoring draws on extensive pre-existing imaging technology to enable high-resolution images to be taken of the build process and can be readily applied to both PBF-LB/M and DED-LB/M processes. Visual light images capture electromagnetic (EM) radiation in the range perceptible to the human eye and thus offer an advantage in being easy to interpret. Metallographic inspection has long relied on the information available in the visible light reflected from the sample to determine the physical properties of metallic surfaces, and as such, visible light images of AM surfaces can similarly provide useful information. Pores, cracks, and geometric deviations are some of the defects that can be detected by visual imaging if they can be resolved by the imaging device. Visual imaging can be carried out at a wide range of resolutions and framerates, as shown in Table 2, generating significant amounts of data, exceeding 5 GB/s in some cases. The high rate of data generation poses significant challenges for any attempt at real-time defect detection using image-fed ML algorithms such as CNNs, which can be computationally expensive, but has been reported in Yuan et al. (2019) by using cropped images to reduce data size.

The distinction between still imaging and video monitoring is somewhat arbitrary, with the primary differences between them relating to their usage. Video feed may be reserved for a human controller to observe the dynamics of the AM process, while images are generally more suited to the analysis and detection methods that will be discussed in "Analysis of in-situ data" section. However, there are some approaches that do receive video data as input to detection algorithms (Yuan et al., 2019) which can make use of the temporal relationships between successive frames.

Like many of the other sensors, visible light cameras can be installed either coaxially to the process beam or in an off-axis configuration.

Coaxial mounting

A coaxial installation takes advantage of the light reflected from the surface back along the process beam, redirecting it via semi-transparent mirrors or filter-mirror combinations to a sensor, shown schematically by Fig. 2a.

Coaxial mounting introduces several constraints on the sensors implemented. Firstly, for a coaxial camera to be mounted, the AM machine must have mounting ports that allow sensors to utilise this light source and is more frequently found in DED-LB/M machines than PBF-LB/M. Secondly, the method of light re-direction inherent to an AM machine will exclude some wavelengths from the sensor (Berumen et al., 2010). As intense laser radiation can be damaging to optical sensors, the exclusion of such wavelengths is generally beneficial, and additional filters may be applied to further ensure exclusion of these wavelengths. However, the impact of excluding wavelengths on sensor response should be carefully considered when designing a monitoring approach.

Further, coaxial monitoring strongly constrains the available field of view to a small region surrounding the process zone as shown in Fig. 2b. The exact area monitored will vary between machines, the working distance, and any nozzle aperture, but is generally a small region of the build surface relative to the entire build area. This may be disadvantageous when the quality of the entire build layer is the desired output, such as when powder spreading inconsistencies are being monitored (Scime & Beuth, 2018a). Alternatively, knowing that the images are localised to the beam spot on the surface makes it simple for the coordinates of the images to be recorded during production, allowing any defects detected to be localised.

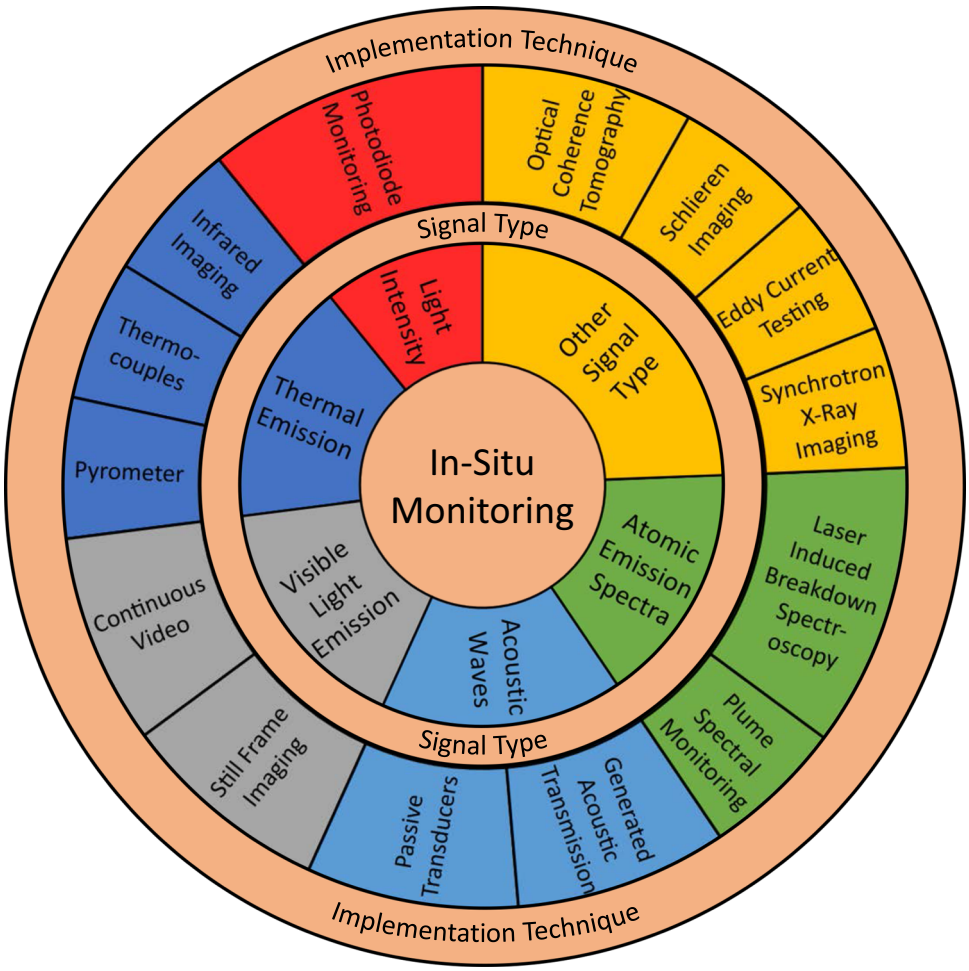

Fig. 1 Radial Map of In-Situ Monitoring Technologies used in Laser-Based Metal AM. The inner circle represents the signal type to be monitored, and the outer circle shows the techniques implemented to monitor the process

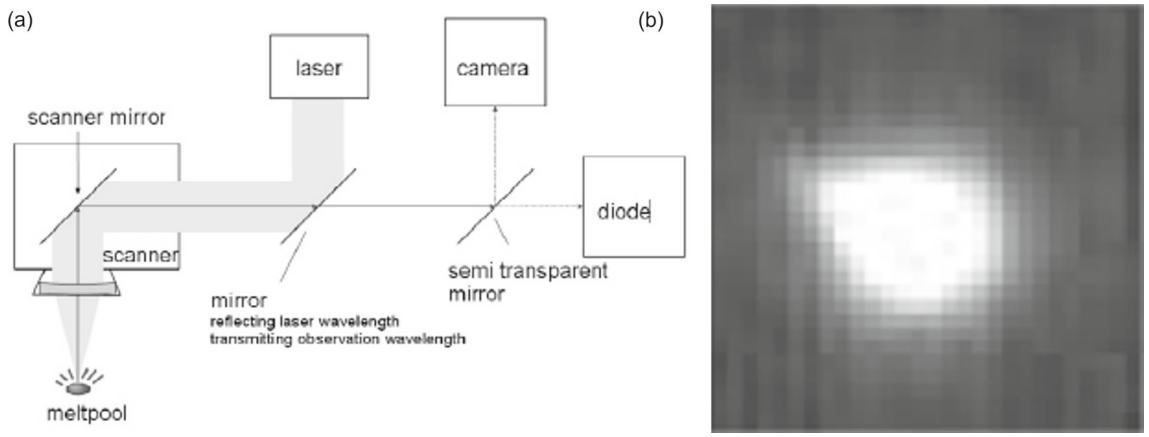

Fig. 2 Coaxial monitoring of the melt pool utilising visible light. **a** Schematic of coaxial monitoring system utilising laser optics and semi-transparent mirrors to direct signal to a camera or diode sensor while removing reflected laser-beam wavelengths from the detected signal (adapted from Berumen et al. (2010)). **b** Coaxial visible light image of melt pool in grayscale; white pixels represent high-intensity light and indicate the area of the melt pool (size scale unavailable) (adapted from Kwon et al. (2020))

Off-axis mounting

Off-axial installation of sensors is achieved by any sensor not coupled to the optical train of the process beam and can either be stationary, as used by Scime and Beuth (2018b), or co-moving with the process zone, as used by Lu et al. (2019). Off-axis installation does not require any specialised design for sensor implementation and allows for more customised installations and thus is equally applicable to PBF-LB/M and DED-LB/M.

Stationary monitoring is the preferred implementation when layer-wise information is the target of a study. Layer-wise imaging, as shown in Fig. 3a, generally occurs only between layer fabrication steps so that the process head does not interfere with the imaging. As indicated earlier, this can be useful in detecting large-scale problems during production, such as the powder spreading faults in Fig. 3b, or thermally-induced part deflection (Scime & Beuth, 2018a). However, the off-axis positioning of the camera imposes a perspective-based distortion which must be accounted for. The difference in distance between points on the build layer and the camera lens can also prevent accurate focus on different areas of the build, further limiting the applicability for detecting smaller defects. Depending on available room in the build chamber, stationary monitoring may rely on small, robust sensors, such as the Fibre Bragg Grating in Shevchik et al. (2018), or observation windows transparent to the monitored signal as in McCann et al. (2021).

Co-moving approaches can allow for constant focus on, or adjacent to, the process zone, similarly to coaxial monitoring, as demonstrated by two different spectral monitoring studies by Chen et al. (2018) and Lednev et al. (2019) respectively. In Lu et al. (2019), a co-moving setup comprising two off-axis cameras was used to measure the melt pool height and solidified cladding height to determine the evolution of internal stresses during solidification. A line-laser was directed at the cladding surface to aid in the detection of the profile and height of the final layer, as shown in Fig. 4. This approach takes advantage of the angled perspective to calculate the height of the cladding layer.

Thermal emission

Thermal emission monitoring refers to the use of the infrared (IR) portion of the EM spectrum, which provides information on surface temperatures of the build during part production. Thermal processes are key to metal AM, and the complex heat transfer throughout the part and into the surrounding media influences the microstructure, residual stress, and thermal deformation states of the part. Monitoring the temperature characteristics of the part provides some information on these states, and potential defects, such as delamination, spatter and porosity (Yang et al., 2020).

Thermal monitoring for AM can be achieved using thermal cameras and pyrometers, with both off-axis, Fig. 5a, and coaxial, Fig. 5c, arrangements. This has allowed thermal monitoring to be successfully applied to both PBF-LB/M and DED-LB/M processes. Thermocouples can also be used but have far less versatility for process monitoring purposes. Thermal cameras are similar to visual light cameras in implementation, but images display temperature distributions in false colour, as shown in Fig. 5b. These images can contain information relating to thermal gradients and structural features that can be interpreted by image-based ML algorithms, such as CNNs, similarly to visible light images. Changes to heat flow due to delamination or cracks can be resolved in these images, and have been successfully identified through ML algorithms, as shown in Fig. 5e. Information such as thermal gradients, temperature extremes, and geometric information can also be extracted from thermal images and then fed to vector-based ML algorithms, such as SVMs, as shown by Ye et al. (2022). However, the pixel resolution of thermal cameras is generally lower than visible light cameras, see Table 2, limiting the detection capabilities for small features.

Thermal cameras come in two primary classes: photon, or thermal detectors. Photon detectors convert IR photons directly to electrical signals and are sensitive to the order of 20 mK and can achieve a higher framerate than thermal detectors. However, they are expensive and require cooling to cryogenic temperatures to avoid thermal noise. Conversely, thermal detectors absorb heat directly, triggering a proportional electrical signal, and achieve a temperature sensitivity on the order of 40 mK (Gade & Moeslund, 2014). In Laser AM, temperatures can vary by up to 1000 K/mm (Thompson et al., 2015), as in Fig. 5b, making sensitivities in the mK range unnecessary for accurate monitoring. As such, thermal detectors may be sufficient for most in-situ thermal monitoring cases.

One major limitation of thermal cameras is their inability to directly measure the absolute temperature of a surface. Objects emit EM radiation in relation to their temperatures, and while the determination of absolute temperature is simple for perfect emitters (blackbodies), few physical objects act as blackbodies. Instead, most have an emissivity value less than one that varies with temperature and physical state in relationships that are rarely established. The assumption of a graybody is that the emissivity is some constant between 0 and 1 and is often made so that the absolute temperature can be estimated (Gade & Moeslund, 2014). However, this assumption cannot account for the variation in emissivity with the large temperature ranges experienced in metal AM, which can result in large errors when reporting the absolute temperature of a surface (Farshidianfar et al., 2016; Felice, 2008). Methods for determining the absolute temperature have been developed but require an independent temperature

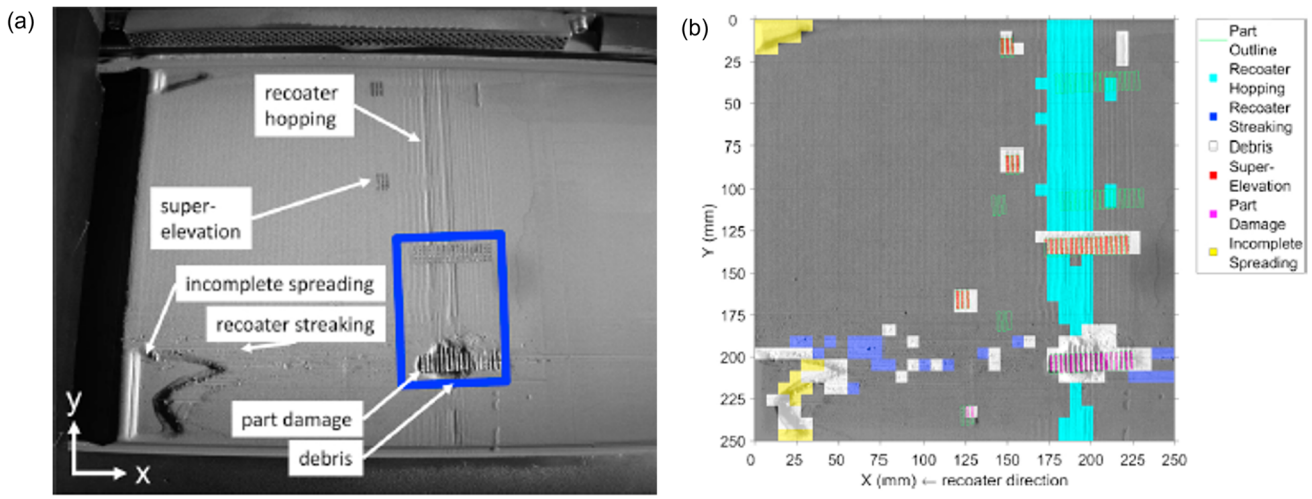

Fig. 3 Stationary, off-axis monitoring of powder bed (adapted from Scime and Beuth (2018b)). **a** Visible light image of powder bed interpreted by a Multi-scale CNN (MsCNN) to identify the powder-spreading defects detected in **b**

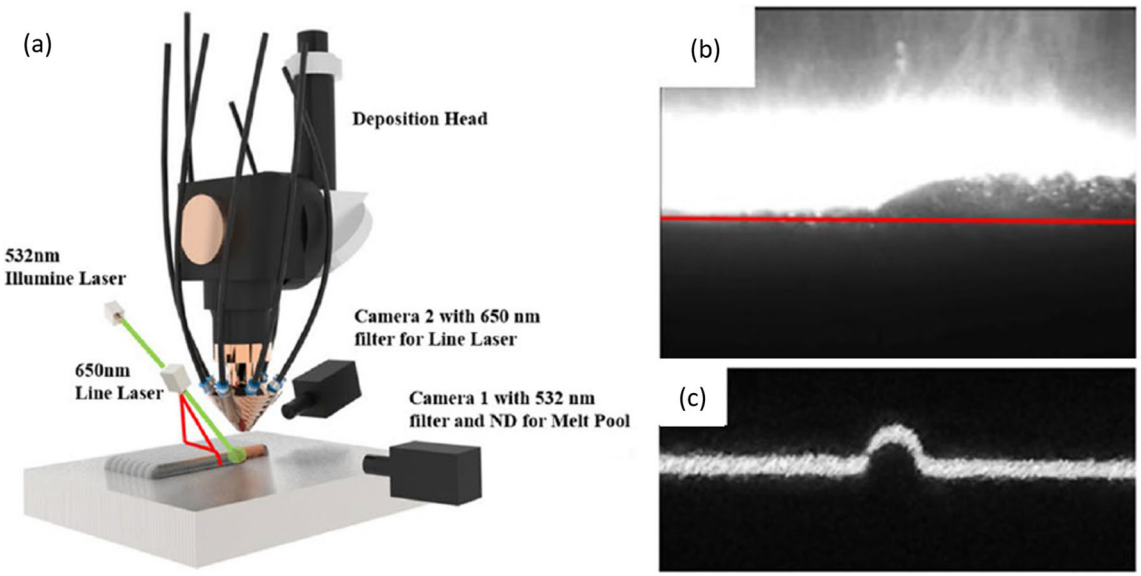

Fig. 4 Off-axis monitoring of DED-LB/M/316L process with two co-moving visual cameras (adapted from Lu et al. (2019)). **a** Experimental set-up of DED-LB/M with horizontal camera for measuring melt pool height and angled camera for measuring cladding height with line laser. **b** Melt pool image from horizontal camera. **c** Track illuminated by line laser and imaged from angled camera

measurement for the same material (Griffith et al., 1998). Calibrations can be performed for a point, such as identifying the melt pool boundary and assuming the temperature at that point to be the solidus temperature (Gould et al., 2020); however, this still imposes a graybody assumption on the material.

Pyrometry is another technique used for monitoring the temperature of a surface and can be used independently or in conjunction with thermal cameras. Pyrometers are generally considered point sensors, Table 2, and are often targeted at monitoring the melt pool temperature (Thompson et al., 2015), Fig. 5c, but some can provide a degree of spatial resolution (Khanzadeh et al., 2018). Pyrometers monitor the intensity of light emitted from a surface in one or more IR wavelengths to determine temperature (Felice, 2008), producing a time-varying signal like that in Fig. 5d. The captured data can then be used to train ML algorithms, such as the unsupervised Self-Organising Map (SOM) used for ML porosity prediction by Khanzadeh et al. (2019). If only one band is monitored, then an assumption as to the emissivity of the surface must also be made. Two- or multi-colour pyrometers use the ratio between intensities to estimate the

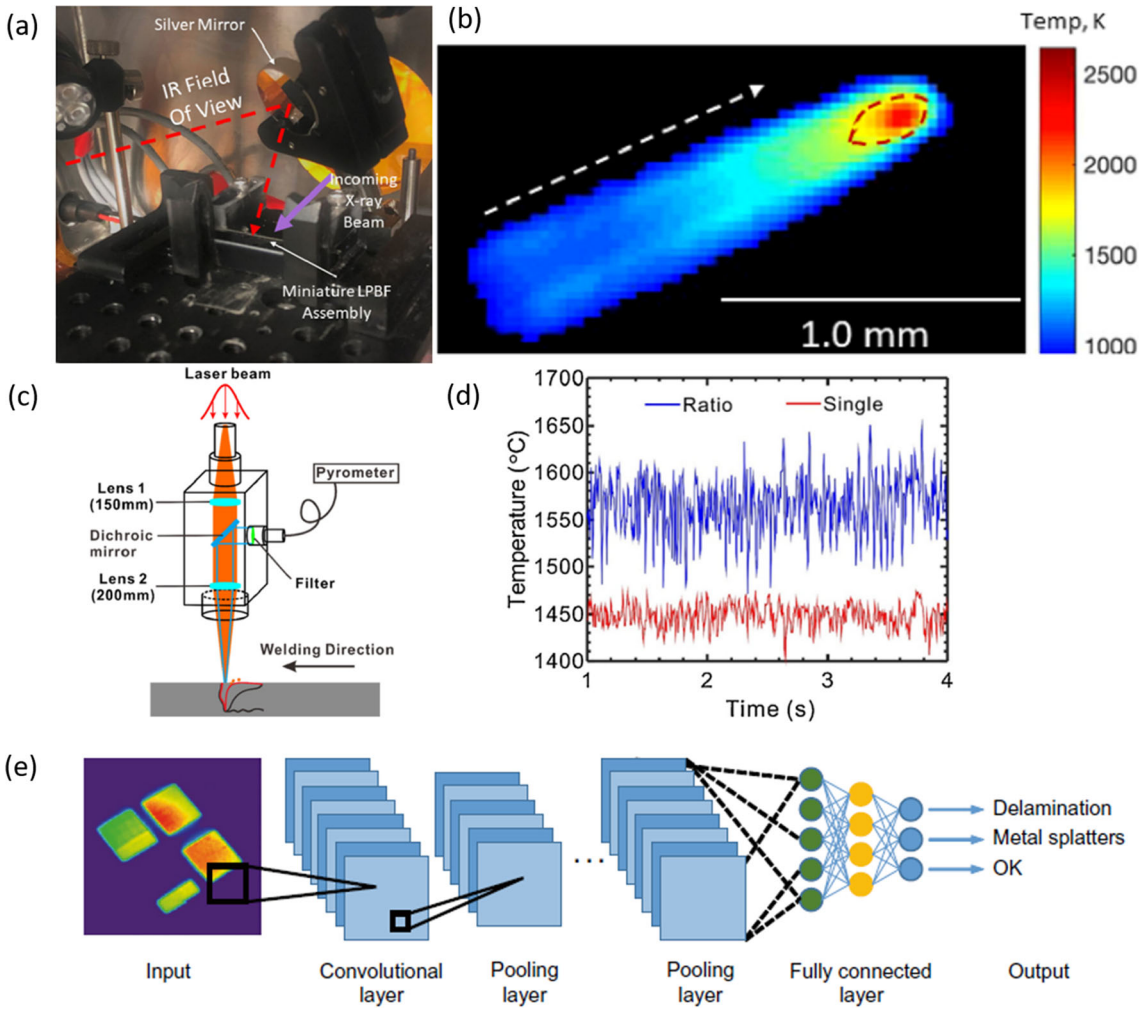

Fig. 5 Thermographic monitoring methods. **a** Specialised experimental setup for thermal and x-ray monitoring of PBF-LB/M process. IR field of view is reflected to the camera by the mirror as indicated. Thermographic image of PBF-LB/M single-track scan shown in **b** with white arrow indicating scan direction, and red dotted circle marking the melt pool boundary. The temperature scale in Kelvin is provided (**a**, **b** adapted from Gould et al. (2020)). **c** Schematic of laser welding process with coaxial pyrometer to monitor melt pool temperature. Temperature response of pyrometer shown in **d** with both dual-colour ratio (blue) and single-colour (red) modes over four seconds (**c**, **d** adapted from Xiao et al. (2020)). **e** An example workflow for a CNN used to predict whether thermal images of PBF-LB/M/H13 builds indicated the presence of delamination, spatter, or were "ok" (adapted from Baumgartl et al. (2020)) (Color figure online)

absolute temperature of the surface and are generally considered emissivity independent (Xiao et al., 2020). However, even these pyrometers are most effective if the emissivity slope (ratio of emissivity at different wavelengths) is calibrated for the material being measured, as described in Rezaeifar and Elbestawi (2021).

Light intensity

Photodiodes monitor the intensity of light emitted within a narrow wavelength band, as shown in Fig. 6a, and are similar to pyrometers in application and construction, the primary difference being that a photodiode is not sensitive only to IR light. In practice, pyrometers are often photodiodes equipped with an optical filter to isolate the IR wavelengths to determine temperature (Grasso & Colosimo, 2017; Zavalov et al., 2019). Photodiodes function by converting incident light to an electrical current, producing a time-varying intensity signal, Fig. 6b, and therefore do not provide spatial resolution. These intensity signals contain multiple features in the data that can be extracted and correlated to make predictions on the final part quality, as demonstrated by the Gaussian Mixture Model in Fig. 6c and d (Okaro et al., 2019).

Atomic emission spectra

The high temperatures in laser AM can cause a small portion of the alloy to evaporate and form a plasma. Within

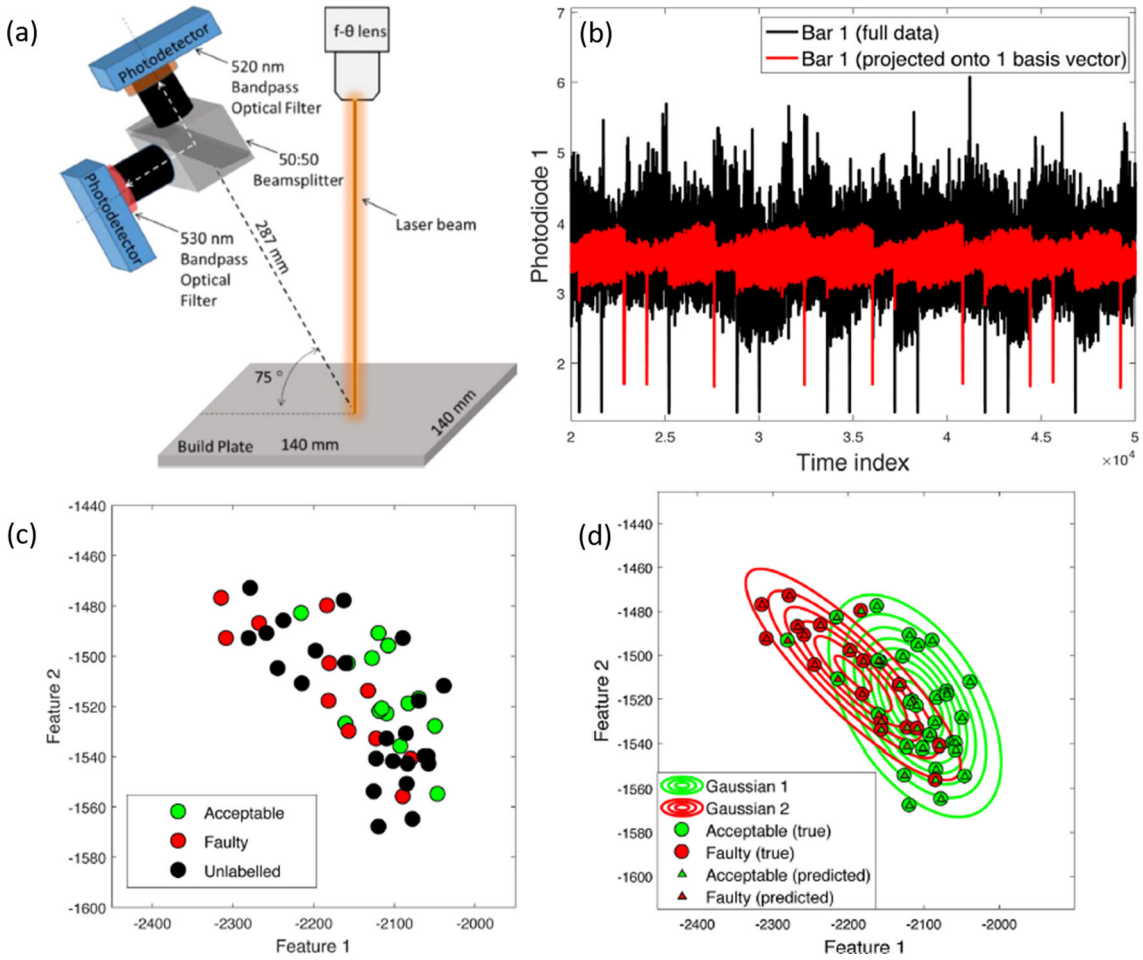

Fig. 6 Acquisition of in-situ photodiode data. **a** Schematic of off-axis collection of melt pool light intensity at 520 nm and 530 nm with two photodiodes (photodetectors) using a beamsplitter (adapted from Montazeri et al. (2020)). **b** Coaxial photodiode time-intensity signal from PBF-LB/M/Inconel 718 in raw (black) and compressed (red) formats. **c** Features extracted from the photodiode data were correlated, and a semi-supervised learning technique was applied to result in the prediction shown in **d** (**b**, **c** and **d** adapted from Okaro et al. (2019)) (Color figure online)

this plasma excited atoms emit photons resulting in an emission spectrum, also called an optical emission spectrum (OES), characteristic of the atomic species and excitation states present (Bartkowiak, 2010; Chen et al., 2018; Valdiande et al., 2021). The characteristic nature of these spectral signals enables the identification of species present in the plasma, which is not possible using the visible or thermal monitoring methods previously discussed.

Spectral monitoring has been adapted to AM processes in both active and passive forms. Active monitoring is achieved by using a probe laser to evaporate a small sample of the surface, forming a plasma which is then analysed by a spectrometer in a process known as Laser-Induced Breakdown Spectroscopy (LIBS) (Hussain & Gondal, 2013). The LIBS system designed by Lednev et al. (2019) was mounted off-axially and used to measure the elemental composition of the melt pool as it was formed in powder DED-LB/M/Ni,Fe,B,Si, Fig. 7a. The LIBS required off-line calibration but could detect both low- and high-atomic weight elements without impacting the deposition properties. This system would not easily be adaptable to PBF-LB/M processes as it requires an extra module to be installed in a position close to the build surface, which is generally incompatible with the optical train of an PBF-LB/M system.

Passive spectral monitoring utilises a spectrometer to analyse the plasma formed by the primary laser beam. This approach is simpler and requires less additional equipment, as in Fig. 7b, whilst also increasing the flexibility of monitoring. This form of monitoring has been reported in both PBF-LB/M and DED-LB/M systems and installed in both coaxial and off-axial arrangements (Bartkowiak, 2010; Chen et al., 2018; Lough et al., 2020; Montazeri et al., 2020; Shin & Mazumder, 2018). However, this method depends on the plasma produced by the primary laser, which is optimised to

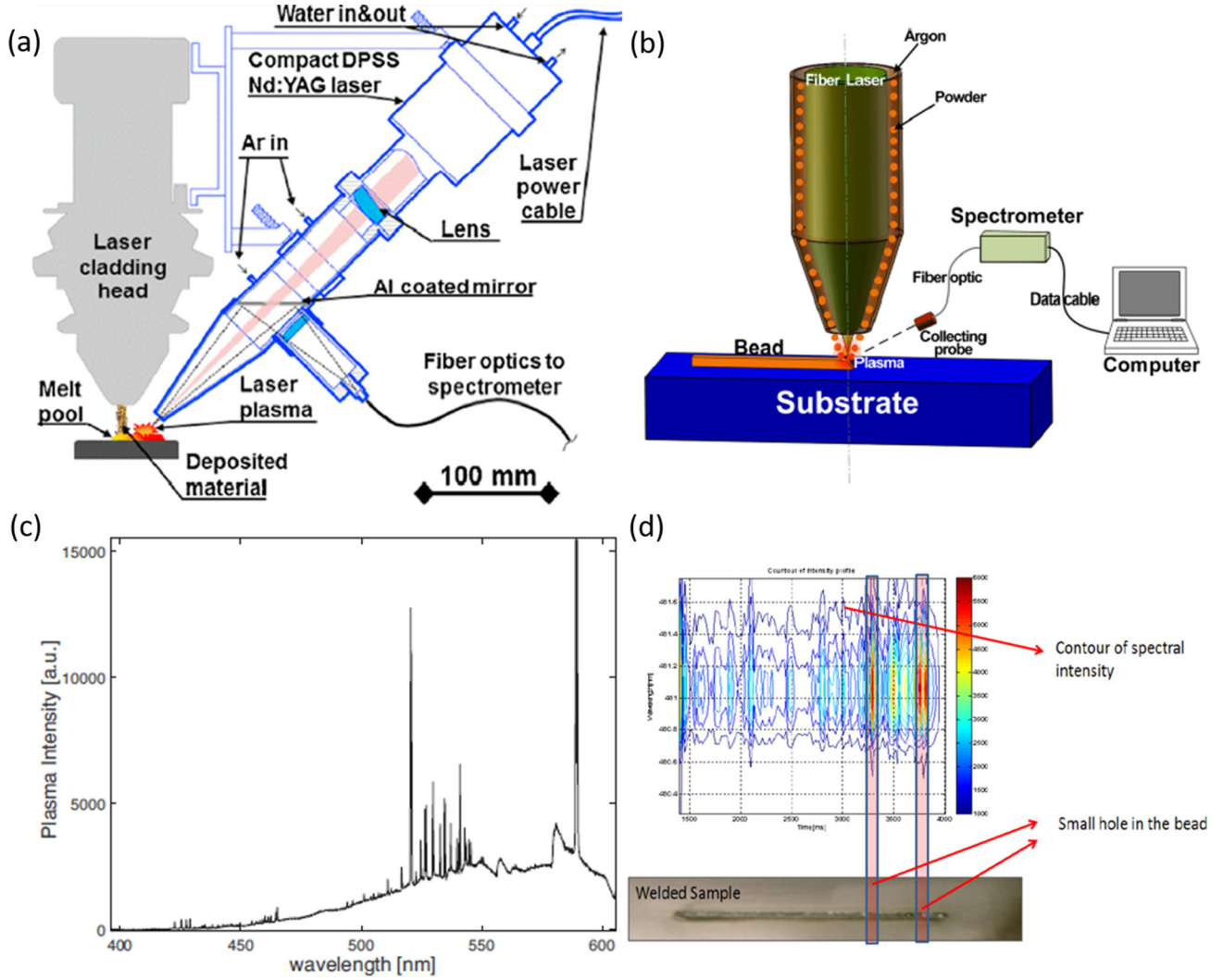

Fig. 7 In-situ spectroscopic monitoring of laser-metal AM. **a** Laser-Induced Breakdown Spectroscopy (LIBS) probe mounted to the side of an existing DED-LB/M head. The probe monitors the deposited material as it is laid down by the deposition head (adapted from Lednev et al. (2019)). **b** Off-axis spectrometer monitoring the melt pool plume generated by the DED-LB/M/316L process (adapted from Chen et al. (2018)). **c** Example spectrogram recorded using a melt pool-focused spectrometer to monitor the deposit formed by an DED-LB/M/Metco 42C process (adapted from Ya et al. (2015)). **d** Changes in the spectral intensity recording for a weld line correlate well with the occurrence of defects in the weld bead (adapted from Mazumder (2015))

produce the highest quality component rather than the best plasma for analysis, and can also distort the laser focus and affect build quality (Xiao et al., 2020).

The spectroscopic signals, such as that shown in Fig. 7c, enable the accurate detection of elements in the plasma, down to the parts per million level in the case of LIBS (Hussain & Gondal, 2013). The concentration of elements in the plasma will be closely related to that of the surface but will not necessarily be identical (Shin & Mazumder, 2018), as some elements will evaporate at lower temperatures than others. These signals can then be utilised by ML algorithms, such as the Support Vector Regression (SVR) method used by Song et al. (2017) to predict on the composition of the deposited alloy.

Elemental concentrations are generally determined from the ratios of spectral line intensities of different elements (Shin & Mazumder, 2018), but the spectroscopic signal can also be acquired for other purposes. In Montazeri et al. (2020) line to continuum intensity ratios were recorded for training several ML algorithms to predict the severity of pores within the consolidated track. Other studies (Chen et al., 2018; Mazumder, 2015) have shown that variations in line

intensities and ratios can be analysed to identify changes in process conditions that result in defect formation, such as in Fig. 7d, and possibly leveraged in process control systems.

Acoustic waves

Instead of EM radiation, acoustic monitoring relies on the propagation of sound waves to provide information on the build quality. Recording and analysis of acoustic emission is a well-established monitoring technique for the detection of cracks, corrosion onset and condition verification in conventional industry (Canumalla et al., 1994; Manthei & Plenkers, 2018; Zhang et al., 2019b) and has recently been adapted to laser AM. Acoustic monitoring systems can be either passive in nature, detecting only the sound waves created during the manufacturing process itself, or they can be active in nature, generating an acoustic wave to travel through the target and return to the receiver. Defects such as pores, cracks or unmelted powders within a part can alter the transmission of these waves, resulting in variations that can be detected in the signals recorded (Shevchik et al., 2018).

In metal AM, passive acoustic sensors measure the vibrations that may travel through the air or through the manufactured part itself, depending on sensor placement. In Shevchik et al. (2018), a Fibre Bragg Grating detector measured the acoustic waves transmitted through the air during PBF-LB/M/CL 20ES, as shown in Fig. 8a and b. This type of sensor is advantageous because the sensor unit is relatively cheap in comparison to other sensors, such as piezoelectric sensors. They are available in a range of configurations, are extremely sensitive to acoustic vibrations and can be installed in an unobtrusive location in the build chamber as shown in Shevchik et al. (2018). In this work, the data was extracted in the form of a spectrograph and used to train a variation of CNN algorithm to detect the severity of pore density in the part. In Koester et al. (2018) and Koester et al. (2019), a method for implementing an array of acoustic transducers below the build plate for DED-LB/M/Ti6Al4V was presented, Fig. 8c and d. Similarly, in Rieder et al. (2016), and more recently in Eschner et al. (2020), ultrasonic transducers were attached to the underside of an PBF-LB/M build platform and the signal was monitored during the production of parts with designed defects or differing densities.

Ultrasonic sensors are an example of an active sensor that has been used extensively in failure analysis, fatigue monitoring and traditional manufacturing for many years. Through the implementation of laser-generated acoustic waves (Dixon et al., 2011), this sensor technology has become applicable to laser AM as well (Hirsch et al., 2017; Pieris et al., 2019). In Smith et al. (2016), a secondary laser generates short pulses of heat on the surface causing thermal expansion and acoustic waves to be transmitted across the sample surface. A detection laser (Hirsch et al., 2017; Smith et al., 2016), or acoustic transducer (Dixon et al., 2011) trained on the surface is able to read the acoustic waves generated on the surface and detect variations that would indicate the presence of a defect. This apparatus and resultant surface map are shown in Fig. 8e and f. This map can be used as input for a CNN-based algorithm, as was shown by Williams et al. (2018) for the identification of porosity in PBF-LB/M.

However, this type of sensor cannot investigate the melt pool region of the build during production. Further, most PBF-LB/M build chambers have little available space for integrating additional equipment within the chamber. To overcome this limitation, Smith et al. (2016) suggested that it may be possible to integrate this sensor to the existing optical train of PBF-LB/M machines, implying that measurements may be conducted between layers using the existing laser guidance equipment.

Emerging approaches

Several other approaches have been developed for in-situ monitoring of Laser AM. However, these methods are either best suited for research purposes or are not yet practical for production-scale monitoring.

Synchrotron X-ray monitoring and Schlieren imaging are helpful research tools for laser AM and can provide valuable insights into the phenomena occurring during laser processing. Synchrotron X-ray monitoring allows the melt pool region to be imaged in high resolution, revealing the dynamics of the processing (Chen et al., 2020; Gould et al., 2020; Guo et al., 2018; Martin et al., 2019; Richter et al., 2019; Zhao et al., 2017). Schlieren Imaging investigates the fluid dynamics of the laser plume and build chamber, revealing how the AM process is affected by its environment (Bidare et al., 2018a, 2018b). Both techniques require specialised experimental setup, which cannot be readily adapted to production scale processes.

Optical Coherence Tomography (OCT) and Inline Coherent Imaging (ICI) monitoring allow the surface of a part to be inspected and indicate the effects of processing parameters (Kanko et al., 2016) and scanning strategy (DePond et al., 2018) on surface roughness. Eddy current testing (ECT) is used to detect cracks and sub-surface defects within metals (Ghoni et al., 2014) and has been proposed as a method for in-situ monitoring of AM processes (Du et al., 2018; Kobayashi et al., 2019). Currently, OCT and ICI have been minimally explored for in-situ monitoring, and ECT has only recently been deployed for in-situ monitoring of PBF-LB/M/AlSi10Mg by Spurek et al. (2022). As these detection systems undergo further exploration for laser metal AM, it is likely that ML will be applied to assist in classification and prediction of samples, but there is little literature exploring this at this point.

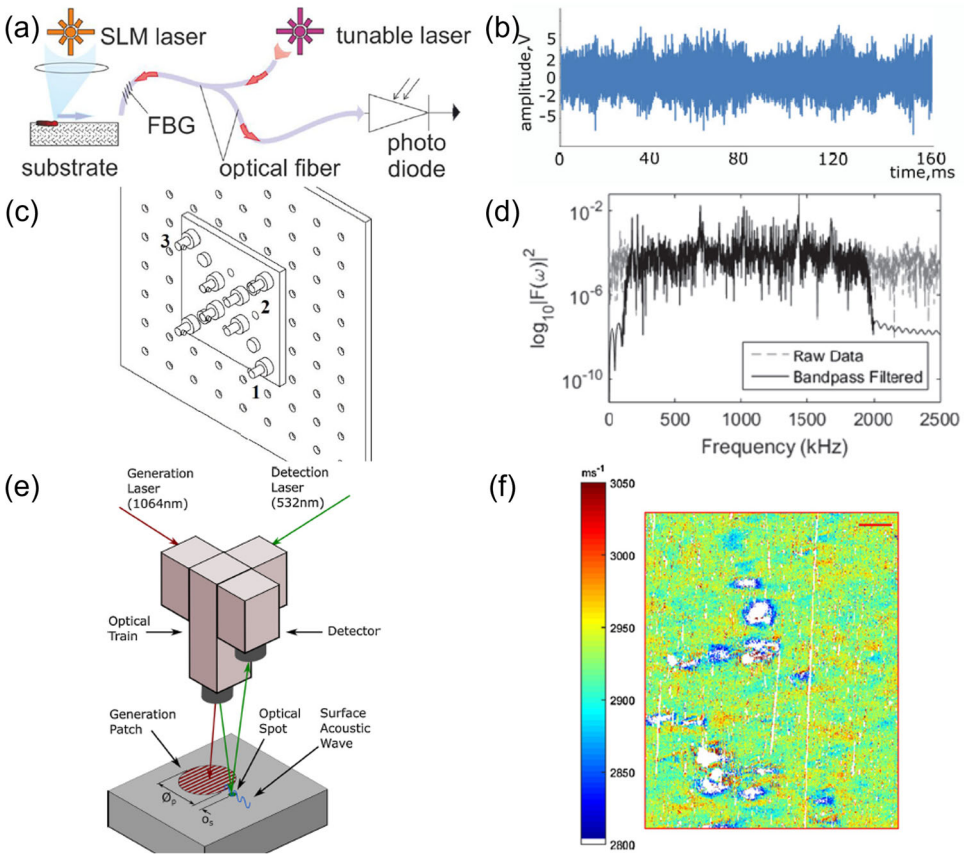

Fig. 8 Examples of acoustic monitoring methods. **a** Schematic of Fibre Bragg Grating sensor in which vibrations alter the diffraction pattern of the tuneable laser in the fibre optic cable (adapted from Shevchik et al. (2018)). This signal is carried to a photodiode, and the signal shown in **b** is recorded (adapted from Wasmer et al. (2019)). **c** Contact acoustic transducers (numbered 1–3) attached below the build plate for a DED-LB/M/Ti6Al4V process and **d** an example recorded waveform showing unprocessed (grey) and bandpass filtered (black) signal (**c**, **d** adapted from Koester et al. (2018)). **e** Schematic of Spatially Resolved Acoustic Spectroscopy (SRAS) monitoring instrument scanning across the surface of a workpiece. The generation laser creates surface acoustic waves (SAW), which a detection laser can then probe to determine the speed of the SAW. **f** An acoustic velocity map (scale bar is 250 μm) recorded by the detector portion of the SRAS instrument. Defects are shown in white, where the SAW does not travel (**e**, **f** adapted from Smith et al. (2016))

Sensor summary

Table 2 has been constructed to provide a guide to the ranges reported within studies on in-situ monitoring of laser AM. As such, the values indicated are not to be taken as a comprehensive range of possible operating values for the monitoring instruments themselves. Where possible, ranges have been listed using comparable units, but some exceptions were necessary due to differences in reporting. It should also be noted that many sensors listed in this table have notable gaps for the rate of data generation and for the resolution of data sources. These gaps indicate that there is room for improvement when reporting on experimental parameters and data acquisition of monitoring sensors. While the rate at which data from the in-situ monitoring technique is generated may be unimportant for monitoring-focused studies, it is relevant to the implementation of real-time data analysis. Hence, where possible the data rate has been included or calculated using Eq. 1 from Berumen et al. (2010),

$$Bytes/s = \frac{x_{pixels} \times y_{pixels} \times bd \times frame\ rate}{8} \quad (1)$$

where *bd* is the bit-depth (assumed as 8-bit for unspecified grayscale images) and the standard 1024 bytes per kB is used.

As shown, data capture rates can be substantial, on the order of several GB/s, causing difficulties for real-time processing. As will be discussed further in "Machine learning to predict anomalies" section, real-time detection of defects requires the recorded data to be processed at high speeds, not yet achievable with full-sized image data. Hence, large data is frequently "down-sampled" in other ML applications to lower the frame size, resolution, or frequency of transferred data (e.g., every tenth datum may be transferred, or images cropped). Alternatively, certain features can be extracted

Table 2 Summary of sensor capabilities as reported by studies utilising in-situ monitoring technologies for Laser-based metal AM

Signal type	Sensor	Monitoring target	Mounting	Data format	Data rate (Theoretical)	Resolution	Sampling rates	References
Visible light	Still Frames Continuous video	Melt pool Build surface	Coaxial and off-axis	Image frames (0.02–0.8 MP)	125 MB/s–5.86 GB/s	14–340 μm/px	60 Hz–100 kHz	Bidare et al. (2018a), Furumoto et al. (2013), Kwon et al. (2020), Li et al. (2022), Lu et al. (2019), Scime and Beuth (2018a), Yang et al. (2020), Yuan et al. (2019)
Thermal emission	Pyrometer	Small point (e.g., melt pool)	Coaxial and off-axis	Temp-Time series; Image frames (5200 px)	–	3.96–21 μm/px	9.3 Hz–100 kHz	Furumoto et al. (2013), Mitchell et al. (2020), Stockman et al. (2019), Xiao et al. (2020)
	Infrared imaging	Melt pool Build surface	Coaxial and Off-axis	Image frames (256–0.3 MP)	~ 6.6 MB/s	30–760 μm/px	50 Hz–90 kHz	Baumgartl et al. (2020), Gould et al. (2020), Jalalahmadi et al. (2019), Ramirez (2019), Yang et al. (2020)
	Thermocouples	Installation point	Base plate	Temp-Time series	–	2 locations	5 Hz	Denlinger et al. (2016)
Light intensity	Photodiode	Small point (e.g., melt pool)	Coaxial and off-axis	Voltage–Time series	~ 115 KB/layer	–	100 kHz–1 MHz	Gaikwad et al. (2020), Montazeri et al. (2020), Okaro et al. (2019)
Atomic emission spectra	Plume-focused spectrometer	Plume area	Coaxial and off-axis	Intensity-wavelength plots	–	Spectral Res: 0.05–1 nm	Sampling time: 1 ms–70 ms	Chen et al. (2018), Lough et al. (2020), Montazeri et al. (2019), Shin and Mazumder (2018), Song et al. (2017), Wang et al. (2020)

Table 2 (continued)

Signal type	Sensor	Monitoring target	Mounting	Data format	Data rate (Theoretical)	Resolution	Sampling rates	References
	Laser-induced breakdown spectroscopy	Probe focus point	Off-axis	Intensity-wavelength plots	–	0.5 mm spot diameter	10 Hz	Lednev et al. (2019)
Acoustic Waves	Passive transducers	Build surface/volume	Build chamber housing or build plate	Waveforms; Spectrograms; Voltage–Time series	–	Temporal: < 1 ns Spatial: 4 locations	200 kHz–10 MHz	Koester et al. (2018), Koester et al. (2019), Shevchik et al. (2018), Wasmer et al. (2019), Wasmer et al. (2018a, 2018b), Ye et al. (2018a, 2018b)
	Active transducers or sensors		Moveable head	Waveforms	–	~ 100 μm (Depth sensitivity: ~ 24 μm)	2 kHz	Smith et al. (2016)
Other signal types	Optical coherence tomography	Entire build plate (250 × 250 mm)	Coaxial and off-axis	Height map	–	100–125 μm/px Point spread function width: 7–20 μm	10 Hz–200 kHz	DePond et al. (2018), Kanko et al. (2016), Yadav et al. (2020)
	Schlieren imaging camera	Build volume	Horizontal outside build area	Image frames (0.2–0.4 MP)	5.97–14.6 GB/s	–	16–80 kHz	Bidare et al. (2018a, 2018b)
	Eddy current probe	Build surface	Recoater blade	Impedance-time series	–	Point spacing: 0.26 mm	375 Hz	Spurek et al. (2022)
	Synchrotron X-ray detector	Region around melt pool	Horizontal outside build area	Image frames (0.1–1.0 MP)	–	1–6.6 μm/px	200 Hz–1 MHz	Chen et al. (2020), Gould et al. (2020), Guo et al. (2018), Leung et al. (2018), Martin et al. (2019), Richter et al. (2019), Zhao et al. (2017)

from images (such as melt pool diameter) and used in vector-fed ML algorithms to mitigate the data size concerns.

Analysis of in-situ data

The purpose of in-situ monitoring is to collect process-relevant data simultaneous to fabrication, which can then be used to determine the state of the component throughout production. In general, this is useful for understanding the condition of the final product. Numerical modelling is also often employed in the AM industry to predict the final state of AM components, investigate physical processes, and correlate and reveal underlying physics. For instance, multi-physics models have advanced the theoretical comprehension of gas flow (Chen & Yan, 2020), melt pool motion (He & Mazumder, 2007), pore formation (Bayat et al., 2019), heat flow (Bayat et al., 2019; He & Mazumder, 2007; Nickel et al., 2001) and more within the AM field. However, one of the most significant limitations to its application in AM is the difficulty in accurately capturing multi-physics phenomena across different scales. By contrast, detecting defects or anomalous states during production allows for individual assessments of components as they are built, negating many of the difficulties associated with accurately capturing statistical variation and unexpected deviations.

Machine learning to predict anomalies

ML models are trained on data acquired during manufacture and can be applied to predict the state of a build based on part-specific data, learning relationships between input data and output states independently. However, the potential of real-time detection of defects by use of ML is still being investigated, and most studies are currently focused on determining the maximal detection accuracies possible. Once trained, these ML approaches can process input data at high speeds, less than 0.1 s per image in the case of the three-class weld quality classifier using a CNN model demonstrated by Li et al. (2020). Algorithms that work on smaller "feature" style data instead of full images or datasets, such as the SVM, have been reported to allow for real-time composition monitoring (Song et al., 2017) and defect detection (Liu et al., 2019) using spectroscopic and video monitoring, respectively, in DED-LB/M processes. However, the inference time, which is the time required to classify a new input datum, is rarely reported on, especially in comparison to the data acquisition rate, which can be easily in the kHz range, as seen in Table 2.

Further optimisation of ML algorithms and data handling may reduce inference times to the point when real-time defect classification becomes possible for algorithms with more complex data. To this end, down-sampling of data may prove necessary by significantly reducing the size of data to be processed. Reducing the dimensions of image data by cropping to regions of interest (Yuan et al., 2019) or reducing resolution can both drastically reduce the amount of data to be processed. There is precedent for achieving high accuracy with low-resolution images. The MNIST (Modified National Institute of Standards and Technology) database, created by Lecun et al. (1998), contains images of handwritten digits at resolutions of 28 × 28 pixels, and ML algorithms have achieved classification accuracies exceeding 99% (Ahlawat et al., 2020). While a simplified example, this suggests that high-resolution imaging at high speeds may not be necessary for accurate defect detection for some defect types in laser AM processes.

Most research currently employs classification-based detection algorithms, labelling data as one of just a few categories as simply as "normal" and "abnormal", or listing up to several defect states and a normal state, as seen in Scime and Beuth (2019). These approaches have reported true positive accuracy rates in the range of roughly 75–95%, with a few claiming to achieve greater than 95%. These results are best conveyed in context, such as using a confusion matrix (see "Appendix 3"), which allows researchers to evaluate the overall performance.

Some investigations use only idealised data for training, such as high-resolution micrographs (Li et al., 2020) or observations of artificial defects (Liu et al., 2019) instead of real-world data. While some authors recognise these limitations and suggest future works to address these shortcomings, not all works demonstrate this. To accurately gauge how the AM process monitoring field is progressing towards timely and accurate defect detection, there must be an increase in the number of studies comparing their results to real-world benchmarks, as is done in other ML fields.

Table 3 provides an analysis of 50 separate studies exploring ML and in-situ monitoring for laser AM processes, all of which have been published from 2017 onwards.

From an inspection of this table, several statistics regarding the spread of topics in the body of literature can be obtained and are shown in Fig. 9.

Of the works reviewed, over 75% apply supervised learning methodologies, with only one study by Wasmer et al. (2019) investigating the use of RL, despite the advancements it has enabled in other fields (discussed in "Discussion and future directions" section). While supervised strategies can be more accurate and easier to interpret than other approaches, real-world data sets for these will be time-consuming and expensive to create. Ground-truth labels must be determined, often manually, then assigned to each training datum. Due to this cost, datasets may be small, biased towards a specific condition and may only allow for simple characterisations. Conversely, unsupervised, and semi-supervised algorithms are designed to work with unlabelled, or partially labelled, datasets. By grouping similar data together, these

Table 3 ML approaches to in-situ monitoring of metal AM processes in fifty separate studies from the body of available literature ('+' indicates a combination of factors, whereas '&' indicates a comparison)

ML category	Model architecture	AM process(es)	Signal type	Data types utilised	Purpose of model	Reference work(s)
Supervised	CNN	PBF-LB/M	Thermal emission	Thermal images	Predict conformity of tensile bars to strength thresholds	Kunkel et al. (2019)
					Delamination and spatter detection	Baumgartl et al. (2020)
					Contour shape detection	Elwarfalli et al. (2019)
			Visible light	Optical images	Laser power prediction	Kwon et al. (2020)
					Detect powder spreading anomalies	Scime and Beuth (2018b)
					Porosity level classification	Li et al. (2021)
					Detect powder spreading anomalies	Westphal and Seitz (2021)
					Weld quality of surface[a]	Zhang et al. (2019a)
				High-speed video segments	Predict average track width and track continuity	Yuan et al. (2018)
			Thermal emission and visible light	Thermal and optical tomographic images[b]	Predict the quality of the melted segment	Ren et al. (2020)
			Acoustic waves	Acoustic signals	Porosity level prediction	Wasmer et al. (2018a, 2018b)
			Light spectra	Hyperspectral images	Surface roughness prediction	Gerdes et al. (2021)
		DED-LB/M, Laser welding	Thermal emission	Thermal images	Dilution estimation (Defect detection	Gonzalez-Val et al. (2020)
		DED-LB/M	Acoustic waves	Wavelet transformed image plots	Detection of different machine operating states	Hossain and Taheri (2021)
	SVM	PBF-LB/M	Thermal emission	Feature 'Fingerprints'	Predict probable defect state from melt pool features	Scime and Beuth (2019)[c]
			Visible light	Optical images	Defect detection	Gobert et al. (2018)
			Light intensity	Photodetector signal + simulated temperature	Prediction of part overhang or bulk	Gaikwad et al. (2020)[d]

Table 3 (continued)

ML category	Model architecture	AM process(es)	Signal type	Data types utilised	Purpose of model	Reference work(s)
		DED-LB/M	Thermal emission	Pyrometer data + simulated temperature	Defect detection	Gaikwad et al. (2020)[d]
			Visible light	Optical images	Track quality prediction	Liu et al. (2019)
			Visible light + Atomic emission spectra	Optical images + Optical emission signatures	Predict severity class for lack of fusion defects	Montazeri et al. (2019)
	CNN & SVM	PBF-LB/M	Visible light	Optical images	Track quality prediction	Zhang et al. (2018)
	CNN & NN	PBF-LB/M	Visible light	Optical images	Defect detection	Snow et al. (2021)
	CNN + Multi-layer perceptron NN	PBF-LB/M	Visible light	Optical images (with wavelet transform and texture analysis)	Classification of processing condition based on energy density	Mojahed Yazdi et al. (2020)
	NN & SVM	PBF-LB/M	Visible light	Optical images	Defect detection	Petrich et al. (2020)
					Hot-spot related defect detection	Bugatti and Colosimo (2021)
	Back propagation NN & SVM & DBN	PBF-LB/M	Visible light	Optical images	Porosity level classification	Li et al. (2022)
	Support vector regression (SVR)	DED-LB/M	Atomic emission spectra	Optical emission signatures	Prediction of aluminium concentration	Song et al. (2017)
	Spectral CNN	PBF-LB/M	Acoustic waves	Acoustic signals[e]	Porosity level prediction	Shevchik et al. (2018, 2019)
	Dynamic segmentation CNN	PBF-LB/M, PBF-EB/M, binder jetting	Visible light	Optical images	Semantic segmentation of anomalies in powder bed	Scime et al. (2020)
	Deep CNN	PBF-LB/M	Visible light	Optical images	Process condition pattern detection	Caggiano et al. (2019)
	SVM & DT & KNN & Linear discriminant (LD) & K-means & NN	PBF-LB/M	Atomic emission spectra	Optical emission signatures	Percentage porosity level	Montazeri et al. (2020)
	Bayesian classifier	PBF-LB/M	Visible light	Optical images	Layer quality classification	Aminzadeh and Kurfess (2019)
	Linear/Quadratic discriminant analysis (LDA & QDA) & DT & KNN & SVM	DED-LB/M	Thermal emission	Pyrometer data	Predict if melt pool characteristics will result in porosity or not	Khanzadeh et al. (2018)
	K-d Tree	PBF-LB/M	Thermal emission	Pyrometry data	Detection of melt pools likely to result in porosity	Mitchell et al. (2020)

Table 3 (continued)

ML category	Model architecture	AM process(es)	Signal type	Data types utilised	Purpose of model	Reference work(s)
	DBN & CNN & Multi-layer perceptron NN	PBF-LB/M	Thermal emission	Thermal images	Classification of melt states	Ye et al. (2018a, 2018b)
	Early stopping NN & Random forest	DED-LB/M	Thermal emission	Pyrometry data	Binary classification of porosity	Behnke et al. (2021)
	Active search + Hyperdimensional computing	PBF-LB/M	Visible light	Optical images	Lack of fusion pore detection	Chen et al. (2021b)
	NN	PBF-LB/M	Visible light + Light intensity + Acoustic waves + Other	Optical images, photodiode intensity, acoustic signals and scan vectors	Defect detection	Petrich et al. (2021)
Unsupervised	Self-organising map (SOM)	DED-LB/M	Thermal emission	Pyrometer data	Predict porosity location	Khanzadeh et al. (2019)
	Bag of words	PBF-LB/M	Visible light	Optical images	Detect powder spreading anomalies	Scime and Beuth (2018a)
					Melt pool feature extraction	Scime and Beuth (2019)[c]
	DBN	PBF-LB/M	Acoustic waves	Acoustic signals	Defect detection	Ye et al. (2018a, 2018b)
	K-means clustering	PBF-LB/M	Visible light	Optical images	Hot-spot related defect detection	Bugatti and Colosimo (2021)
Semi-Supervised	CNN	PBF-LB/M	Visible light	High-speed video segments	Predict average track width and track continuity	Yuan et al. (2019)
				Optical micrographs	Weld quality of surface[a]	Li et al. (2020)
	CNN + RNN	PBF-LB/M	Thermal emission	Thermal images	Build condition classification	Larsen and Hooper (2021)
	KNN	DED-LB/M	Other signal type	Laser profiler point cloud data	Detect surface defects	Chen et al. (2021a)
	K-means clustering + KNN	PBF-LB/M	Other signal type	Optical tomography	Predict hotspots in a layer	Yadav et al. (2020)
	Gaussian mixture model (GMM)	PBF-LB/M	Light intensity	Photodiode intensity signals	Predict conformity of tensile bars to strength threshold	Okaro et al. (2019)
Reinforcement	Q-Learning	PBF-LB/M	Acoustic waves	Acoustic signals[e]	Porosity level classifier	Wasmer et al. (2019)

All studies utilising DED-LB/M were powder-fed, and terminology used in studies has been preserved where possible
[a]These studies utilise an off-line optical micrograph image dataset, known as UB-Moog produced by Moog, Inc., Buffalo, NY (Zhang et al., 2019a)
[b]Simulated sensor data was used in this study
[c]Different aspects of the same study. The Unsupervised model provided the input to the Supervised model
[d]The combination of simulated data and monitored signal is tested on both PBF-LB and DED-LB
[e]Using the same acoustic data from the initial study (Shevchik et al., 2018)

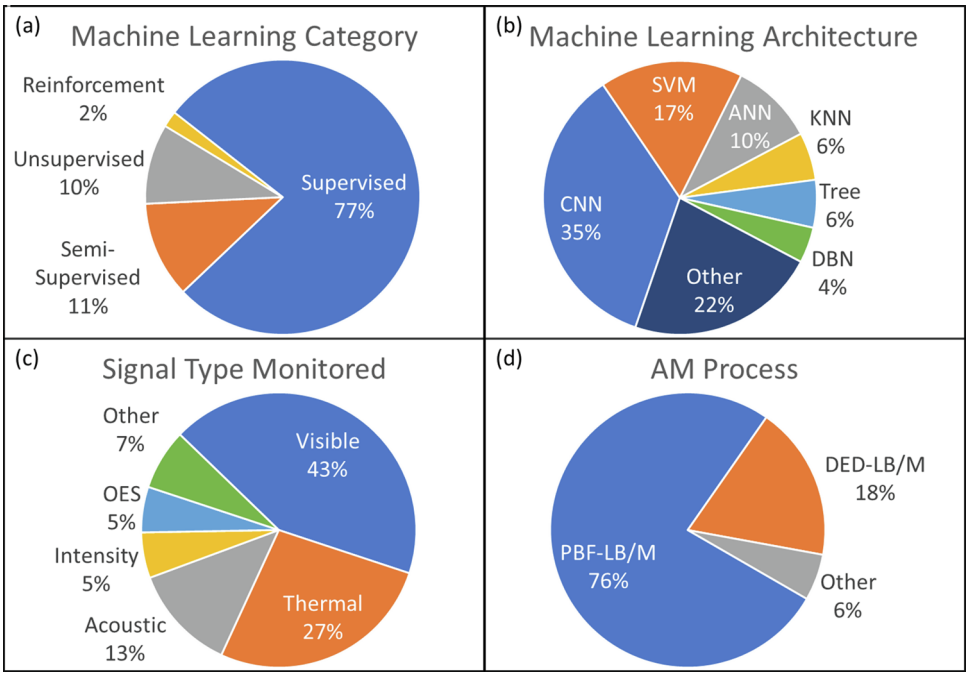

Fig. 9 Prevalence of **a** monitored signal type, **b** ML architecture utilised, **c** ML category employed, and **d** the AM process being monitored for the works reviewed in Table 3. Note: the 'Other' processes included here relate only to non-laser metal AM processes that were a part of a study that did investigate PBF-LB/M or DED-LB/M where Machine Learning and in-situ monitoring were applied similarly to the laser AM process studied

algorithms can learn unexpected features or relationships in the data. Scime and Beuth (2019) used an unsupervised Bag of Words method to group images of samples and found that an expected feature was not detected by the algorithm, while an unexpected feature was.

There is also a strong preference for the collection of visible and thermal emission data, together comprising 70% of all instances in the literature surveyed. Imaging sensors, in both visible and IR bands, can provide spatial resolution from a few micrometres per pixel, allowing for defects and features to be identifiable. This can also allow for multiple features to be identified within individual frames, providing a rich data source for defect detection algorithms. Thermal monitoring, image-based or otherwise, can additionally provide valuable data on thermal history and melt pool condition. However, both thermal and visible light signals are typically limited to surface measurements and can miss indications of sub-surface defects which might instead be detected through other monitoring technologies, such as acoustic sensors.

The preference for visual and thermal data corresponds strongly with the CNN-based and SVM type model architectures, occupying 35% and 17% of all approaches, respectively. Both algorithms are well understood and can be highly informative. CNN algorithms are especially adept at processing image-based data, while SVM algorithms can rapidly process vectorized data, such as temperature–time signals. As typically supervised algorithms, these can be expensive to train, and CNNs additionally require extensive computing resources, proportional to the size of input images. Given the large variety of ML algorithms available, further advancement of other approaches may well provide new insights into the formation of defects and undesirable product states.

Finally, there is a strong tendency towards investigation in PBF-LB/M systems compared to DED-LB/M. Over 75% of studies consider PBF-LB/M systems for their investigations, while just 18% analyse DED-LB/M, with none of those being wire-fed systems. The remainder here is comprised of processes being compared to a laser metal AM within the same study but utilising a relevant approach. It should also be considered that ML implementation in other fields often benefits from transfer learning on similar data sets to improve the robustness of predictions. And while there are instances of transfer learning relying on data from outside of the AM field (Mojahed Yazdi et al., 2020), there are no studies utilising transfer learning between PBF-LB/M and DED-LB/M.

Anomaly detection without machine learning

In many manufacturing processes, signals are monitored in real-time and deviations from a prescribed range of values are considered anomalous. These deviations are often correlated with out-of-control processing that may lead to the formation of a defective product. This approach is different to the application of ML, and typically detects anomalous process conditions rather than individual defects. Additionally, these detection limits are frequently hard-coded and determined from experimentally informed process maps, by operator experience, or from a simulation, not learned from the data as is the case with ML.

The detection of undesirable conditions using process limits has shown some promise as a viable and practical

method. One example is the commercially available CLAMIR (Control for Laser Additive Manufacturing with Infrared imaging) system, a thermographic imaging and control package demonstrated by Ramirez (2019) to monitor and actively modify the dimensions of the melt pool in DED-LB/M manufacturing. A similar approach is described by Chen et al. (2018), where the intensity of different spectral lines was monitored in an DED-LB/M process, and control limits were established based on "normal" operation. Deviations from these control limits were associated with the formation of unwanted deposit or defects. It should be noted, however, that the detections presented in this paper were the result of extreme changes to the process parameters, and therefore did not demonstrate the realistic sensitivity of this method.

Control limit detection of defective states is a comparatively simple method for detecting poor build conditions when contrasted with ML-based detections. Following detection, some studies have exploited Statistical Process Control (SPC) for controlling melt pool size (Ding et al., 2016; Ramirez, 2019), cooling rate (Farshidianfar et al., 2016), and deposition height in Gas Tungsten Arc AM (Xiong et al., 2019; Zhu & Xiong, 2020). Indeed, control limits, and associated SPC of process variables have proven useful in improving consistency and quality in the metal AM industry, but are generally incapable of learning new relationships in data or for detecting individual defects as they occur.

Few studies have compared control limit detection to ML detection of defective production. However, one example by Grasso and Colosimo (2019) has shown that ML algorithms can ameliorate the detection of out-of-control processes over purely statistical control limits. In this study, the authors apply an SVM to improve the region of interest and control chart design over a statistical model they had previously produced (Grasso et al., 2018). The ML-augmented approach enabled earlier detection of out-of-control manufacture and at a significantly reduced time. As control-limit detection and SPC can be considered the current industry standard for in-situ detection and control, comparisons to these in future publications would prove beneficial to the field.

Discussion and future directions

As the AM industry continues to transition from a prototyping and research dominated sector into a commercially viable manufacturing option, demands on quality control and assurance will continue to increase. ML-based defect detection and process monitoring offer a pathway towards the realisation of feedback process control and defect-free products for high-value industries.

The rapid and accurate detection of some defect classes are beginning to be realised in the field of laser metal AM. A recent study by Ren et al. (2023) reported 100% prediction accuracy for keyhole pore detection in PBF-LB/M/Ti6Al4V using supervised machine learning on IR imaging data. This result was made possible through the use of a multiphysics simulation informed by synchrotron X-ray monitoring. Approaches such as this one elucidate the underlying physical phenomena that give rise to the defect formation, therefore providing a physics-informed pathway to process modification and feedback control.

In-situ process control is a new paradigm in AM that seeks to control the process variables, like laser power, to maintain targeted values for monitored signals, such as temperature. Once detected and identified by ML algorithms, defective build conditions could be modified and adapted during production. This potential for closed-loop control is expected to provide a solution to the lack of part consistency in the industry. The currently employed optimisation of process parameters fails to account for stochastic fluctuations and process variations that are well known to cause the formation of undesirable features. Control systems are already common in other industries and allow systems to adapt to these changes, minimising the effects they have on the quality of the product.

Closed-loop process control would introduce several benefits to AM, including reduced waste, minimisation of manufacturing defects, and improved production consistency. There currently exist systems, such as the previously discussed CLAMIR system (Ramirez, 2019), which demonstrate the capability to control the melt pool size in real-time, moving beyond detecting adverse conditions and enabling improved product quality. However, these systems, governed by control limits, are limited to pre-defined responses only and make no diagnosis of potential problems nor offer the possibility for remediation. Alongside the minimisation of non-critical defects, such as pores, that are known to affect the mechanical responses of the final component (Salarian et al., 2020), intelligent ML control systems could give rise to a paradigm of in-process certification, drastically reducing the requirement for extensive quality control testing post-manufacture (Mazumder, 2015).

Furthermore, recent advancements within the ML field have led to the development of programs capable of outperforming human experts in non-analytical circumstances. An RL algorithm called *AlphaGo Zero*, designed to play the board game 'Go' (with more than 10^{575} total possible moves and board configurations (Cai & Wunsch, 2007)), consistently defeats human expert players and other AI-based approaches, and has even developed novel strategies that have since been adopted by human players (Sutton & Barto, 2018). The number of processing parameters and materials available to laser AM is on the order of several dozen (Silbernagel et al., 2019; Spears & Gold, 2016), and these parameters are typically non-discrete in nature. This makes the possibility of

mapping out the material-process space in any AM category similarly impractical to mapping out the game space of 'Go' to identify a solution to every situation. It is likely that similarly inspired RL approaches can be adapted to the AM field to learn their own corrective actions after detecting defects or process deviations, and that existing ML models could be used to train these algorithms (Yeung et al., 2020). Such self-learning programs could result in adaptive process control by machines capable of observing multiple signals and correcting deviations in real-time. Such capability would result in a dramatic rise in AM components' quality and a corresponding increase in the uptake of AM processes by high-value industries.

Various ML approaches have been applied to defect detection and build classification in laser metal AM, using a wide variety of data structures and process monitoring technologies. Thermal and visible light imaging methods are among the most implemented technologies, providing large amounts of image data to CNNs for classification of defects. These sensors are known to provide valuable information on the process conditions, but they also create large volumes of data with storage and transmission difficulties. Vector-fed algorithms, such as SVMs, Decision trees and ANNs, make use of features extracted from processing signals and can utilise data from spectrometers, photodiodes, and acoustic transducers, as well as images. These sensors can provide unique benefits and inform on different aspects of the build process that cannot be deduced from image data alone. Several other sensor technologies are being investigated for process monitoring, but these are either best suited to research tasks or require further development before they can be widely adopted and will likely foster further ML investigations.

Recent studies have demonstrated the capabilities of ML algorithms to detect the presence of defects or undesirable build conditions from various forms of sensor data, including visual images, spectrographic intensity ratios and acoustic signals. Supervised ML approaches, such as CNNs and SVMs, have dominated the available literature regarding the detection of undesirable states from sensor signals, providing for relatively high accuracy in simple classification tasks. Some approaches have even been reported as capable of providing classifications in real-time through the use of simpler networks, downsized data or refined feature selections. As research continues to advance the use of ML-based detection systems toward real-time and closed-loop control of AM processes, there are several critical aspects of the literature that will reflect the progress made:

1. Reporting of inference rates between studies investigating the applicability of ML for the detection of defects is not yet consistent. This is needed to directly compare different approaches and help drive networks' development for real-time detection.
2. The spatial resolution and data generation rates of monitoring sensors are rarely described in detail. These relate directly to systems' physical detection limits and the applicability of the generated data for rapid evaluation necessary for closed-loop control.
3. Prediction results of ML algorithms are typically framed only within the context of each study, making it difficult to compare performance across studies. The use of a universal benchmark would foster the development of more robust ML systems for wider AM use.
4. The current range of predicted outcomes from many current ML approaches is limited to simple two- or three-class predictions. Quantitative outputs, such as dilution ratios and morphological predictions, will provide more detailed information on the building process.
5. There is a strong tendency toward using supervised ML approaches, particularly using CNN and SVM algorithms, for the investigation of PBF-LB/M processes and monitoring by visual or thermal cameras. The exploitation of other available technologies and monitoring strategies may improve process understanding or result in stronger predictive performance of ML approaches.
6. Improvements in data handling, transfer, and conversion to useable formats for ML algorithms will need to be made as the development of real-time detection in closed-loop process control grows.

Acknowledgements This research has been financially supported by RMIT University and CSIRO. The authors would also like to acknowledge the support of the Advanced Manufacturing Precinct (AMP) at RMIT University.

Funding Open Access funding enabled and organized by CAUL and its Member Institutions.

Declarations

Competing interests The authors have no competing interests to declare that are relevant to the content of this article.

Open Access This article is licensed under a Creative Commons Attribution 4.0 International License, which permits use, sharing, adaptation, distribution and reproduction in any medium or format, as long as you give appropriate credit to the original author(s) and the source, provide a link to the Creative Commons licence, and indicate if changes were made. The images or other third party material in this article are included in the article's Creative Commons licence, unless indicated otherwise in a credit line to the material. If material is not included in the article's Creative Commons licence and your intended use is not permitted by statutory regulation or exceeds the permitted use, you will need to obtain permission directly from the copyright holder. To view a copy of this licence, visit http://creativecommons.org/licenses/by/4.0/.

Appendixes

Appendix 1: Abbreviations

Abbreviation	Definition
AI	Artificial Intelligence
AM	Additive Manufacturing
ANN/NN	Artificial Neural Network
CLAMIR	Control for Laser Additive Manufacturing with Infrared imaging
CNN	Convolutional Neural Network
DBN	Deep Belief Network
DED	Directed Energy Deposition
DIC	Digital Image Correlation
DL	Deep Learning
DLD	Directed Lased Deposition
DT	Decision Tree
EB	Electron beam
ECT	Eddy Current Testing
EM	Electromagnetic
FGM	Functionally Graded Material
GMM	Gaussian Mixture Model
HIP	Hot Isostatic Pressing
ICI	Inline Coherent Imaging
IR	Infrared
KNN	K-Nearest Neighbours
LB	Laser beam
LD/LDA	Linear Discriminant/Linear Discriminant Analysis
LENS	Laser Engineered Net Shaping
LIBS	Laser-Induced Breakdown Spectroscopy
LMD	Laser Metal Deposition
LOF	Lack of Fusion
ML	Machine Learning
MNIST	Modified National Institute of Standards and Technology
MP	Megapixels
OCT	Optical Coherence Tomography
OES	Optical Emission Spectrum
PBF	Powder Bed Fusion
PCA	Principal Component Analysis
QDA	Quadratic Discriminant Analysis
RBM	Restricted Boltzmann Machine
RF	Random Forest
RL	Reinforcement Learning
SAW	Surface Acoustic Wave
SOM	Self-Organising Map
SPC	Statistical Process Control
SRAS	Spatially Resolved Acoustic Spectroscopy
SVM	Support Vector Machine
SVR	Support Vector Regression
XCT	X-ray Computed Tomography

Appendix 2: Categories of machine learning

Within the field of Machine Learning (ML), there are four primary categories of learning styles: supervised learning, unsupervised learning, semi-supervised learning, and reinforcement learning. Supervised learning refers to approaches that use fully-labelled data; that is, the data provided to the algorithm has a pre-determined correct answer. The algorithm then inspects the data and over many training iterations, learns to identify patterns in the data that correspond to the correct answer (Lecun et al., 2015). Construction of such a dataset can be extremely time-consuming and expensive, especially when that requires micro X-ray computed tomography (XCT), human inspection or destructive testing to determine the existence or severity of defects. As larger datasets frequently result in improved ML performance, this can limit the practicality of supervised learning approaches. The convolutional neural network (CNN) is an example of a highly successful supervised algorithm that has been used extensively in Additive Manufacturing (AM) for defect detection and part classification (Gonzalez-Val et al., 2020; Kunkel et al., 2019).

Unsupervised learning, by contrast, has no pre-defined label for the data. Instead, the algorithm recognises similarities between subsets of the data and groups these together. A human operator may then inspect the groups and allocate a label to that grouping. One example of this is the Bag of Words algorithm, utilised by Scime and Beuth (2019), where images were grouped by features, and then correlated with similar feature images of known conditions. The authors were able to categorise several different defect states by this method, but they also discovered that one of the expected defect categories, severe keyholing, was not identified by this method, while another unexpected category, spattering, was identified. The unsupervised approach has the advantage of reducing the time and cost of constructing a dataset whilst also having the potential to discover unexpected correlations. However, it is worth noting that supervised approaches can be simpler to evaluate and interpret.

Semi-supervised learning utilises a combination of these two data structures, grouping unlabelled data with similar data that is labelled. By implementing this strategy, the advantages of both supervised and unsupervised learning are combined. Semi-supervised learning can be more accurate than purely unsupervised training, as demonstrated using a

CNN model by Yuan et al. (2019), while it can be significantly easier and cheaper to assemble the dataset than it is for purely supervised learning. Studies have also demonstrated that using unlabelled data in addition to labelled data acquired during production can result in increased prediction accuracy (Li et al., 2020; Okaro et al., 2019).

Instead of attempting to group or classify data provided to it, a reinforcement learning algorithm aims to achieve an overall goal by interacting with its environment through the exploration of different actions available to it. When a model effects a change that causes the environment to move towards the desired state, a reward is provided to it, encouraging further actions that promote that desired state (Sutton & Barto, 2018). Reinforcement methods have so far been limited in the AM monitoring field, but one study by Wasmer et al. (2019) demonstrated it for predicting the quality of laser beam powder bed fusion (PBF-LB) components. This approach applied a Q-Learning algorithm to learn the relationships between clips of acoustic data and the resultant porosity level. The authors presented this research as a feasibility study that achieved lower accuracies than their supervised approaches (Shevchik et al., 2018; Shevchik et al., 2019; K. ; K), but that they expected to show improvement with further optimisation in the future.

Appendix 3: Confusion matrix

A confusion matrix, such as that shown in Fig. 10 is a common method for illustrating the performance of a predictive ML algorithm. In this example, of all input data or samples that are belong to Condition A, 95% of them are predicted correctly, while 2% and 3% are predicted to belong to conditions B and C, respectively. Hence, the diagonal cells show the "true positive" rate for each condition. This example illustrates that the true positive prediction is lowest for condition B, and that this condition is more likely to be incorrectly predicted as condition C than condition A. This can show that the algorithm may have some difficulty differentiating these categories or that the data provided may be unbalanced (Fig. 10).

Prediction / Ground Truth	Condition A	Condition B	Condition C
Condition A	0.95	0.02	0.03
Condition B	0.07	0.75	0.18
Condition C	0.05	0.03	0.92

Fig. 10 Example of a normalised, three-class confusion matrix

References

Ahlawat, S., Choudhary, A., Nayyar, A., Singh, S., & Yoon, B. (2020). Improved handwritten digit recognition using convolutional neural networks (CNN). *Sensors, 20*(12), 3344. https://www.mdpi.com/1424-8220/20/12/3344

Aminzadeh, M., & Kurfess, T. R. (2019). Online quality inspection using Bayesian classification in powder-bed additive manufacturing from high-resolution visual camera images. *Journal of Intelligent Manufacturing, 30*(6), 2505–2523. https://doi.org/10.1007/s10845-018-1412-0

Bartkowiak, K. (2010). Direct laser deposition process within spectrographic analysis in situ. *Physics Procedia, 5*, 623–629. https://doi.org/10.1016/j.phpro.2010.08.090

Baumgartl, H., Tomas, J., Buettner, R., & Merkel, M. (2020). A deep learning-based model for defect detection in laser-powder bed fusion using in-situ thermographic monitoring. *Progress in Additive Manufacturing*. https://doi.org/10.1007/s40964-019-00108-3

Bayat, M., Thanki, A., Mohanty, S., Witvrouw, A., Yang, S., Thorborg, J., Tiedje, N. S., & Hattel, J. H. (2019). Keyhole-induced porosities in laser-based powder bed fusion (L-PBF) of Ti_6Al_4V: High-fidelity modelling and experimental validation. *Additive Manufacturing, 30*, 100835. https://doi.org/10.1016/j.addma.2019.100835

Behnke, M., Guo, S., & Guo, W. (2021). Comparison of early stopping neural network and random forest for in-situ quality prediction in laser based additive manufacturing. *Procedia Manufacturing, 53*, 656–663. https://doi.org/10.1016/j.promfg.2021.06.065

Bentley, J. L. (1975). Multidimensional binary search trees used for associative searching. *Communications of the ACM, 18*(9), 509–517. https://doi.org/10.1145/361002.361007

Berumen, S., Bechmann, F., Lindner, S., Kruth, J.-P., & Craeghs, T. (2010). Quality control of laser- and powder bed-based Additive Manufacturing (AM) technologies. *Physics Procedia, 5*, 617–622. https://doi.org/10.1016/j.phpro.2010.08.089

Bidare, P., Bitharas, I., Ward, R. M., Attallah, M. M., & Moore, A. J. (2018a). Fluid and particle dynamics in laser powder bed fusion. *Acta Materialia, 142*, 107–120. https://doi.org/10.1016/j.actamat.2017.09.051

Bidare, P., Bitharas, I., Ward, R. M., Attallah, M. M., & Moore, A. J. (2018b). Laser powder bed fusion in high-pressure atmospheres. *International Journal of Advanced Manufacturing Technology, 99*(1–4), 543–555. https://doi.org/10.1007/s00170-018-2495-7

Biegler, M., Elsner, B. A. M., Graf, B., & Rethmeier, M. (2020). Geometric distortion-compensation via transient numerical simulation for directed energy deposition additive manufacturing. *Science and Technology of Welding and Joining*. https://doi.org/10.1080/13621718.2020.1743927

Bourell, D. L., Leu, M. C., & Rosen, D. W. (2009). *Roadmap for additive manufacturing: Identifying the future of freeform processing* (pp. 11–15). The University of Texas at Austin.

Brandão, A. D., Gumpinger, J., Gschweitl, M., Seyfert, C., Hofbauer, P., & Ghidini, T. (2017). Fatigue properties of additively manufactured $AlSi_{10}Mg$-surface treatment effect. *Procedia Structural Integrity, 7*, 58–66.

Brandt, M. (2017). The role of lasers in additive manufacturing. In M. Brandt (Ed.), *Laser additive manufacturing* (pp. 1–18). Woodhead Publishing. https://doi.org/10.1016/B978-0-08-100433-3.02001-7

Bugatti, M., & Colosimo, B. M. (2021). Towards real-time in-situ monitoring of hot-spot defects in L-PBF: A new classification-based method for fast video-imaging data analysis. *Journal of Intelligent Manufacturing*. https://doi.org/10.1007/s10845-021-01787-y

Caggiano, A., Zhang, J., Alfieri, V., Caiazzo, F., Gao, R., & Teti, R. (2019). Machine learning-based image processing for on-line

defect recognition in additive manufacturing. *CIRP Annals, 68*(1), 451–454. https://doi.org/10.1016/j.cirp.2019.03.021

Cai, X., & Wunsch, D. C. (2007). Computer go: A grand challenge to AI. In W. Duch & J. Mańdziuk (Eds.), *Challenges for computational intelligence* (pp. 443–465). Springer. https://doi.org/10.1007/978-3-540-71984-7_16

Campbell, C., & Ying, Y. (2011). *Learning with support vector machines*. Morgan & Claypool.

Canumalla, S., Pangborn, R. N., Tittmann, B. R., & Conway, J. C., Jr. (1994). Acoustic emission for in situ monitoring in metal-matrix composite processing. *Composites Science and Technology, 52*(4), 607–614. https://doi.org/10.1016/0266-3538(94)90043-4

Carlton, H. D., Haboub, A., Gallegos, G. F., Parkinson, D. Y., & MacDowell, A. A. (2016). Damage evolution and failure mechanisms in additively manufactured stainless steel. *Materials Science and Engineering: A, 651*, 406–414. https://doi.org/10.1016/j.msea.2015.10.073

Chen, B., Yao, Y., Tan, C., Huang, Y., & Feng, J. (2018). A study on spectral characterization and quality detection of direct metal deposition process based on spectral diagnosis. *International Journal of Advanced Manufacturing Technology, 96*(9–12), 4231–4241. https://doi.org/10.1007/s00170-018-1889-x

Chen, H., & Yan, W. (2020). Spattering and denudation in laser powder bed fusion process: multiphase flow modelling. *Acta Materialia*. https://doi.org/10.1016/j.actamat.2020.06.033

Chen, L., Yao, X., Xu, P., Moon, S. K., & Bi, G. (2021a). Rapid surface defect identification for additive manufacturing with in-situ point cloud processing and machine learning. *Virtual and Physical Prototyping, 16*(1), 50–67. https://doi.org/10.1080/17452759.2020.1832695

Chen, R., Imani, M., & Imani, F. (2021b). Joint active search and neuromorphic computing for efficient data exploitation and monitoring in additive manufacturing. *Journal of Manufacturing Processes, 71*, 743–752. https://doi.org/10.1016/j.jmapro.2021.09.048

Chen, Y., Clark, S. J., Sinclair, L., Leung, C. L. A., Marussi, S., Connolley, T., Magdysyuk, O. V., Atwood, R. C., Baxter, G. J., & Jones, M. A. (2020). In situ and operando X-ray imaging of directed energy deposition additive manufacturing. arXiv preprint arXiv:2006.09087.

Cooper, D., Thornby, J., Blundell, N., Henrys, R., Williams, M. A., & Gibbons, G. (2015). Design and manufacture of high performance hollow engine valves by Additive Layer Manufacturing. *Materials & Design, 69*, 44–55. https://doi.org/10.1016/j.matdes.2014.11.017

de Oliveira, U., Ocelík, V., & De Hosson, J. T. M. (2006). Residual stress analysis in Co-based laser clad layers by laboratory X-rays and synchrotron diffraction techniques. *Surface and Coatings Technology, 201*(3–4), 533–542. https://doi.org/10.1016/j.surfcoat.2005.12.011

DebRoy, T., Mukherjee, T., Wei, H. L., Elmer, J. W., & Milewski, J. O. (2020). Metallurgy, mechanistic models and machine learning in metal printing. *Nature Reviews Materials*. https://doi.org/10.1038/s41578-020-00236-1

Denlinger, E. R., Jagdale, V., Srinivasan, G. V., El-Wardany, T., & Michaleris, P. (2016). Thermal modeling of Inconel 718 processed with powder bed fusion and experimental validation using in situ measurements. *Additive Manufacturing, 11*, 7–15. https://doi.org/10.1016/j.addma.2016.03.003

DePond, P. J., Guss, G., Ly, S., Calta, N. P., Deane, D., Khairallah, S., & Matthews, M. J. (2018). In situ measurements of layer roughness during laser powder bed fusion additive manufacturing using low coherence scanning interferometry. *Materials & Design, 154*, 347–359. https://doi.org/10.1016/j.matdes.2018.05.050

Ding, Y., Warton, J., & Kovacevic, R. (2016). Development of sensing and control system for robotized laser-based direct metal addition system. *Additive Manufacturing, 10*, 24–35. https://doi.org/10.1016/j.addma.2016.01.002

Dixon, S., Burrows, S. E., Dutton, B., & Fan, Y. (2011). Detection of cracks in metal sheets using pulsed laser generated ultrasound and EMAT detection. *Ultrasonics, 51*(1), 7–16. https://doi.org/10.1016/j.ultras.2010.05.002

Du, W., Bai, Q., Wang, Y., & Zhang, B. (2018). Eddy current detection of subsurface defects for additive/subtractive hybrid manufacturing. *International Journal of Advanced Manufacturing Technology, 95*(9–12), 3185–3195. https://doi.org/10.1007/s00170-017-1354-2

du Plessis, A., & Macdonald, E. (2020). Hot isostatic pressing in metal additive manufacturing: X-ray tomography reveals details of pore closure. *Additive Manufacturing, 34*, 101191. https://doi.org/10.1016/j.addma.2020.101191

du Plessis, A., Yadroitsava, I., & Yadroitsev, I. (2020). Effects of defects on mechanical properties in metal additive manufacturing: A review focusing on X-ray tomography insights. *Materials and Design, 187*, 108385. https://doi.org/10.1016/j.matdes.2019.108385

Elambasseril, J., Lu, S. L., Ning, Y. P., Liu, N., Wang, J., Brandt, M., Tang, H. P., & Qian, M. (2019). 3D characterization of defects in deep-powder-bed manufactured Ti–6Al–4V and their influence on tensile properties. *Materials Science and Engineering A, 761*, 138031. https://doi.org/10.1016/j.msea.2019.138031

Elwarfalli, H., Papazoglou, D., Erdahl, D., Doll, A., & Speltz, J. (2019). In situ process monitoring for laser-powder bed fusion using convolutional neural networks and infrared tomography. In *Proceedings of the IEEE national aerospace electronics conference, NAECON*.

Eschner, N., Weiser, L., Häfner, B., & Lanza, G. (2020). Classification of specimen density in Laser Powder Bed Fusion (L-PBF) using in-process structure-borne acoustic process emissions. *Additive Manufacturing, 34*, 101324. https://doi.org/10.1016/j.addma.2020.101324

Farshidianfar, M. H., Khajepour, A., & Gerlich, A. (2016). Real-time control of microstructure in laser additive manufacturing. *International Journal of Advanced Manufacturing Technology, 82*(5–8), 1173–1186. https://doi.org/10.1007/s00170-015-7423-5

Felice, R. (2008). Pyrometry for liquid metals. *Advanced Materials & Processes, 166*(7), 31–33.

Fu, Y., Downey, A. R. J., Yuan, L., Zhang, T., Pratt, A., & Balogun, Y. (2022). Machine learning algorithms for defect detection in metal laser-based additive manufacturing: A review. *Journal of Manufacturing Processes, 75*, 693–710. https://doi.org/10.1016/j.jmapro.2021.12.061

Furumoto, T., Ueda, T., Alkahari, M. R., & Hosokawa, A. (2013). Investigation of laser consolidation process for metal powder by two-color pyrometer and high-speed video camera. *CIRP Annals - Manufacturing Technology, 62*(1), 223–226. https://doi.org/10.1016/j.cirp.2013.03.032

Gade, R., & Moeslund, T. B. (2014). Thermal cameras and applications: A survey. *Machine Vision and Applications, 25*(1), 245–262. https://doi.org/10.1007/s00138-013-0570-5

Gaikwad, A., Yavari, R., Montazeri, M., Cole, K., Bian, L., & Rao, P. (2020). Toward the digital twin of additive manufacturing: Integrating thermal simulations, sensing, and analytics to detect process faults. *IISE Transactions, 52*(11), 1204–1217. https://doi.org/10.1080/24725854.2019.1701753

Gardner, M. W., & Dorling, S. R. (1998). Artificial neural networks (the multilayer perceptron)—A review of applications in the atmospheric sciences. *Atmospheric Environment, 32*(14), 2627–2636. https://doi.org/10.1016/S1352-2310(97)00447-0

Gerdes, N., Hoff, C., Hermsdorf, J., Kaierle, S., & Overmeyer, L. (2021). Hyperspectral imaging for prediction of surface roughness in laser powder bed fusion. *International Journal of Advanced Manufacturing Technology, 115*(4), 1249–1258. https://doi.org/10.1007/s00170-021-07274-1

Ghoni, R., Dollah, M., Sulaiman, A., & Mamat Ibrahim, F. (2014). Defect characterization based on eddy current technique: Technical review. *Advances in Mechanical Engineering, 2014*, 182496. https://doi.org/10.1155/2014/182496

Gibson, I., Rosen, D. W., & Stucker, B. (2014). *Additive manufacturing technologies* (Vol. 17). Springer.

Girelli, L., Tocci, M., Gelfi, M., & Pola, A. (2019). Study of heat treatment parameters for additively manufactured AlSi10Mg in comparison with corresponding cast alloy. *Materials Science and Engineering A, 739*, 317–328. https://doi.org/10.1016/j.msea.2018.10.026

Gobert, C., Reutzel, E. W., Petrich, J., Nassar, A. R., & Phoha, S. (2018). Application of supervised machine learning for defect detection during metallic powder bed fusion additive manufacturing using high resolution imaging. *Additive Manufacturing, 21*, 517–528. https://doi.org/10.1016/j.addma.2018.04.005

Gonzalez-Val, C., Pallas, A., Panadeiro, V., & Rodriguez, A. (2020). A convolutional approach to quality monitoring for laser manufacturing. *Journal of Intelligent Manufacturing, 31*(3), 789–795. https://doi.org/10.1007/s10845-019-01495-8

Gould, B., Wolff, S., Parab, N., Zhao, C., Lorenzo-Martin, M. C., Fezzaa, K., Greco, A., & Sun, T. (2020). In situ analysis of laser powder bed fusion using simultaneous high-speed infrared and X-ray imaging. *JOM Journal of the Minerals Metals and Materials Society*. https://doi.org/10.1007/s11837-020-04291-5

Grasso, M., & Colosimo, B. M. (2017). Process defects and in situ monitoring methods in metal powder bed fusion: A review. *Measurement Science and Technology, 28*(4), 044005. https://doi.org/10.1088/1361-6501/aa5c4f

Grasso, M., & Colosimo, B. M. (2019). A statistical learning method for image-based monitoring of the plume signature in laser powder bed fusion. *Robotics and Computer-Integrated Manufacturing, 57*, 103–115. https://doi.org/10.1016/j.rcim.2018.11.007

Grasso, M., Demir, A. G., Previtali, B., & Colosimo, B. M. (2018). In situ monitoring of selective laser melting of zinc powder via infrared imaging of the process plume. *Robotics and Computer-Integrated Manufacturing, 49*, 229–239. https://doi.org/10.1016/j.rcim.2017.07.001

Grasso, M., Remani, A., Dickins, A., Colosimo, B., & Leach, R. (2021). In-situ measurement and monitoring methods for metal powder bed fusion—An updated review. *Measurement Science and Technology*. https://doi.org/10.1088/1361-6501/ac0b6b

Griffith, M., Schlienger, M., & Harwell, L. (1998). Thermal behavior in the LENS process. In *Solid freeform fabrication symposium*, United States of America.

Günlük, O., Kalagnanam, J., Li, M., Menickelly, M., & Scheinberg, K. (2021). Optimal decision trees for categorical data via integer programming. *Journal of Global Optimization, 81*(1), 233–260. https://doi.org/10.1007/s10898-021-01009-y

Guo, Q., Zhao, C., Escano, L. I., Young, Z., Xiong, L., Fezzaa, K., Everhart, W., Brown, B., Sun, T., & Chen, L. (2018). Transient dynamics of powder spattering in laser powder bed fusion additive manufacturing process revealed by in-situ high-speed high-energy x-ray imaging. *Acta Materialia, 151*, 169–180. https://doi.org/10.1016/j.actamat.2018.03.036

He, X., & Mazumder, J. (2007). Transport phenomena during direct metal deposition. *Journal of Applied Physics, 101*(5), 053113. https://doi.org/10.1063/1.2710780

Hirsch, M., Patel, R., Li, W., Guan, G., Leach, R. K., Sharples, S. D., & Clare, A. T. (2017). Assessing the capability of in-situ nondestructive analysis during layer based additive manufacture. *Additive Manufacturing, 13*, 135–142. https://doi.org/10.1016/j.addma.2016.10.004

Hossain, M. S., & Taheri, H. (2021). In-situ process monitoring for metal additive manufacturing through acoustic techniques using wavelet and convolutional neural network (CNN). *International Journal of Advanced Manufacturing Technology, 116*(11–12), 3473–3488. https://doi.org/10.1007/s00170-021-07721-z

Hussain, T., & Gondal, M. A. (2013). Laser induced breakdown spectroscopy (LIBS) as a rapid tool for material analysis. *Journal of Physics: Conference Series, 439*, 012050. https://doi.org/10.1088/1742-6596/439/1/012050

Jalalahmadi, B., Liu, J., Rios, J., Slotwinski, J., Peitsch, C., Goldberg, A., & Montalbano, T. (2019). In-process defect monitoring and correction in additive manufacturing of aluminum alloys. In *The Vertical Flight Society - Forum 75: The future of vertical flight - Proceedings of the 75th annual forum and technology display*.

Jayaram, J., Amling, A., Chaudhuri, A., & McMackin, D. (2020). Prime time for additive manufacturing. *Supply Chain Management Review, 24*(2), 36–43.

Kanko, J. A., Sibley, A. P., & Fraser, J. M. (2016). In situ morphology-based defect detection of selective laser melting through inline coherent imaging. *Journal of Materials Processing Technology, 231*, 488–500. https://doi.org/10.1016/j.jmatprotec.2015.12.024

Khairallah, S. A., Anderson, A. T., Rubenchik, A., & King, W. E. (2016). Laser powder-bed fusion additive manufacturing: Physics of complex melt flow and formation mechanisms of pores, spatter, and denudation zones. *Acta Materialia, 108*, 36–45. https://doi.org/10.1016/j.actamat.2016.02.014

Khanzadeh, M., Chowdhury, S., Marufuzzaman, M., Tschopp, M. A., & Bian, L. (2018). Porosity prediction: Supervised-learning of thermal history for direct laser deposition. *Journal of Manufacturing Systems, 47*, 69–82. https://doi.org/10.1016/j.jmsy.2018.04.001

Khanzadeh, M., Chowdhury, S., Tschopp, M. A., Doude, H. R., Marufuzzaman, M., & Bian, L. (2019). In-situ monitoring of melt pool images for porosity prediction in directed energy deposition processes. *IISE Transactions, 51*(5), 437–455. https://doi.org/10.1080/24725854.2017.1417656

Kobayashi, N., Yamamoto, S., Sugawara, A., Nakane, M., Tsuji, D., Hino, T., Terada, T., & Ochiai, M. (2019). Fundamental experiments of eddy current testing for additive manufacturing metallic material toward in-process inspection. *AIP Conference Proceedings, 2102*(1), 070003. https://doi.org/10.1063/1.5099803

Koester, L. W., Taheri, H., Bigelow, T. A., Bond, L. J., & Faierson, E. J. (2018). In-situ acoustic signature monitoring in additive manufacturing processes. In *AIP conference proceedings.*

Koester, L. W., Taheri, H., Bond, L. J., & Faierson, E. J. (2019). Acoustic monitoring of additive manufacturing for damage and process condition determination. In *AIP conference proceedings*.

Kunkel, M. H., Gebhardt, A., Mpofu, K., & Kallweit, S. (2019). Quality assurance in metal powder bed fusion via deep-learning-based image classification. *Rapid Prototyping Journal, 26*(2), 259–266. https://doi.org/10.1108/RPJ-03-2019-0066

Kwon, O., Kim, H. G., Kim, W., Kim, G., & Kim, K. (2020). A convolutional neural network for prediction of laser power using melt-pool images in laser powder bed fusion. *IEEE Access, 8*, 23255–23263. https://doi.org/10.1109/ACCESS.2020.2970026

Larsen, S., & Hooper, P. A. (2021). Deep semi-supervised learning of dynamics for anomaly detection in laser powder bed fusion. *Journal of Intelligent Manufacturing*. https://doi.org/10.1007/s10845-021-01842-8

Le Roux, N., & Bengio, Y. (2008). Representational power of restricted boltzmann machines and deep belief networks. *Neural Computation, 20*(6), 1631–1649. https://doi.org/10.1162/neco.2008.04-07-510

Lecun, Y., Bengio, Y., & Hinton, G. (2015). Deep learning. *Nature, 521*(7553), 436–444. https://doi.org/10.1038/nature14539

Lecun, Y., Bottou, L., Bengio, Y., & Haffner, P. (1998). Gradient-based learning applied to document recognition. *Proceedings of the IEEE, 86*(11), 2278–2324. https://doi.org/10.1109/5.726791

Lednev, V. N., Sdvizhenskii, P. A., Asyutin, R. D., Tretyakov, R. S., Grishin, M. Y., Stavertiy, A. Y., & Pershin, S. M. (2019). In situ multi-elemental analysis by laser induced breakdown spectroscopy in additive manufacturing. *Additive Manufacturing, 25*, 64–70. https://doi.org/10.1016/j.addma.2018.10.043

Leung, C. L. A., Marussi, S., Atwood, R. C., Towrie, M., Withers, P. J., & Lee, P. D. (2018). In situ X-ray imaging of defect and molten pool dynamics in laser additive manufacturing. *Nature Communications, 9*(1), 1355. https://doi.org/10.1038/s41467-018-03734-7

Li, J., Cao, L., Xu, J., Wang, S., & Zhou, Q. (2022). In situ porosity intelligent classification of selective laser melting based on coaxial monitoring and image processing. *Measurement: Journal of the International Measurement Confederation, 187*, 110232. https://doi.org/10.1016/j.measurement.2021.110232

Li, J., Zhou, Q., Huang, X., Li, M., & Cao, L. (2021). In situ quality inspection with layer-wise visual images based on deep transfer learning during selective laser melting. *Journal of Intelligent Manufacturing*. https://doi.org/10.1007/s10845-021-01829-5

Li, X., Jia, X., Yang, Q., & Lee, J. (2020). Quality analysis in metal additive manufacturing with deep learning. *Journal of Intelligent Manufacturing*. https://doi.org/10.1007/s10845-020-01549-2

Liu, T., Huang, L., & Chen, B. (2019). Real-time defect detection of laser additive manufacturing based on support vector machine. *Journal of Physics: Conference Series*.

Loh, G. H., Pei, E., Harrison, D., & Monzón, M. D. (2018). An overview of functionally graded additive manufacturing. *Additive Manufacturing, 23*, 34–44. https://doi.org/10.1016/j.addma.2018.06.023

Lough, C. S., Escano, L. I., Qu, M., Smith, C. C., Landers, R. G., Bristow, D. A., Chen, L., & Kinzel, E. C. (2020). In-situ optical emission spectroscopy of selective laser melting. *Journal of Manufacturing Processes, 53*, 336–341. https://doi.org/10.1016/j.jmapro.2020.02.016

Lu, Y., Sun, G., Xiao, X., & Mazumder, J. (2019). Online stress measurement during laser-aided metallic additive manufacturing. *Scientific Reports, 9*(1), 7630. https://doi.org/10.1038/s41598-019-39849-0

Mahmoud, D., Magolon, M., Boer, J., Elbestawi, M. A., & Mohammadi, M. G. (2021). Applications of machine learning in process monitoring and controls of L-PBF additive manufacturing: A review. *Applied Sciences*, *11*(24), 11910. https://www.mdpi.com/2076-3417/11/24/11910

Malefane, L. B., du Preez, W. B., Maringa, M., & Plessis, A. D. (2018). Tensile and high cycle fatigue properties of annealed TI6AL4V (ELI) specimens produced by direct metal laser sintering. *South African Journal of Industrial Engineering, 29*(3), 299–311. https://doi.org/10.7166/29-3-2077

Manthei, G., & Plenkers, K. (2018). Review on in situ acoustic emission monitoring in the context of structural health monitoring in mines. *Applied Sciences, 8*(9), 1595. https://www.mdpi.com/2076-3417/8/9/1595

Martin, A. A., Calta, N. P., Hammons, J. A., Khairallah, S. A., Nielsen, M. H., Shuttlesworth, R. M., Sinclair, N., Matthews, M. J., Jeffries, J. R., Willey, T. M., & Lee, J. R. I. (2019). Ultrafast dynamics of laser-metal interactions in additive manufacturing alloys captured by in situ X-ray imaging. *Materials Today Advances, 1*, 100002. https://doi.org/10.1016/j.mtadv.2019.01.001

Mazumder, J. (2015). Design for metallic additive manufacturing machine with capability for "certify as you build." *Procedia CIRP, 36*, 187–192.

McCann, R., Obeidi, M. A., Hughes, C., McCarthy, É., Egan, D. S., Vijayaraghavan, R. K., Joshi, A. M., Acinas Garzon, V., Dowling, D. P., McNally, P. J., & Brabazon, D. (2021). In-situ sensing, process monitoring and machine control in Laser Powder Bed Fusion: A review. *Additive Manufacturing, 45*, 102058. https://doi.org/10.1016/j.addma.2021.102058

Meng, L., McWilliams, B., Jarosinski, W., Park, H.-Y., Jung, Y.-G., Lee, J., & Zhang, J. (2020). Machine learning in additive manufacturing: A review. *JOM Journal of the Minerals Metals and Materials Society, 72*(6), 2363–2377. https://doi.org/10.1007/s11837-020-04155-y

Mitchell, J. A., Ivanoff, T. A., Dagel, D., Madison, J. D., & Jared, B. (2020). Linking pyrometry to porosity in additively manufactured metals. *Additive Manufacturing, 31*, 100946. https://doi.org/10.1016/j.addma.2019.100946

Mojahed Yazdi, R., Imani, F., & Yang, H. (2020). A hybrid deep learning model of process-build interactions in additive manufacturing. *Journal of Manufacturing Systems, 57*, 460–468. https://doi.org/10.1016/j.jmsy.2020.11.001

Montazeri, M., Nassar, A. R., Dunbar, A. J., & Rao, P. (2020). In-process monitoring of porosity in additive manufacturing using optical emission spectroscopy. *IISE Transactions, 52*(5), 500–515. https://doi.org/10.1080/24725854.2019.1659525

Montazeri, M., Nassar, A. R., Stutzman, C. B., & Rao, P. (2019). Heterogeneous sensor-based condition monitoring in directed energy deposition. *Additive Manufacturing, 30*, 100916. https://doi.org/10.1016/j.addma.2019.100916

Nickel, A. H., Barnett, D. M., & Prinz, F. B. (2001). Thermal stresses and deposition patterns in layered manufacturing. *Materials Science and Engineering A, 317*(1–2), 59–64. https://doi.org/10.1016/S0921-5093(01)01179-0

Okaro, I. A., Jayasinghe, S., Sutcliffe, C., Black, K., Paoletti, P., & Green, P. L. (2019). Automatic fault detection for laser powder-bed fusion using semi-supervised machine learning. *Additive Manufacturing, 27*, 42–53. https://doi.org/10.1016/j.addma.2019.01.006

Oliveira, J. P., Santos, T. G., & Miranda, R. M. (2020). Revisiting fundamental welding concepts to improve additive manufacturing: From theory to practice. *Progress in Materials Science, 107*, 100590. https://doi.org/10.1016/j.pmatsci.2019.100590

Petrich, J., Gobert, C., Phoha, S., Nassar, A. R., & Reutzel, E. W. (2020). Machine learning for defect detection for PBFAm using high resolution layerwise imaging coupled with post-build CT scans. In *Solid freeform fabrication 2017: Proceedings of the 28th annual international solid freeform fabrication symposium—An additive manufacturing conference*, SFF 2017.

Petrich, J., Snow, Z., Corbin, D., & Reutzel, E. W. (2021). Multi-modal SeNSor fusion with machine learning for data-driven process monitoring for additive manufacturing. *Additive Manufacturing*. https://doi.org/10.1016/j.addma.2021.102364

Pieris, D., Patel, R., Dryburgh, P., Hirsch, M., Li, W., Sharples, S., Smith, R., Clare, A., & Clark, M. (2019). Spatially resolved acoustic spectroscopy towards online inspection of additive manufacturing. *Insight-Non-Destructive Testing and Condition Monitoring, 61*(3), 132–137.

Ramirez, A. B. (2019, January). CLAMIR precisely controls advanced laser manufacturing processes. *Laser Focus World*, *55*(1), 99–100. https://www.clamir.com/wp-content/uploads/2019/01/lfw201901-dl.pdf

Ren, Y. M., Zhang, Y., Ding, Y., Wang, Y., & Christofides, P. D. (2020). Computational fluid dynamics-based in-situ sensor analytics of direct metal laser solidification process using machine learning. *Computers and Chemical Engineering, 143*, 107069. https://doi.org/10.1016/j.compchemeng.2020.107069

Ren, Z., Gao, L., Clark, S. J., Fezzaa, K., Shevchenko, P., Choi, A., Everhart, W., Rollett, A. D., Chen, L., & Sun, T. (2023). Machine learning–aided real-time detection of keyhole pore generation in laser powder bed fusion. *Science, 379*(6627), 89–94. https://doi.org/10.1126/science.add4667

Rezaeifar, H., & Elbestawi, M. A. (2021). On-line melt pool temperature control in L-PBF additive manufacturing. *The International Journal of Advanced Manufacturing Technology*. https://doi.org/10.1007/s00170-020-06441-0

Richter, B., Blanke, N., Werner, C., Parab, N. D., Sun, T., Vollertsen, F., & Pfefferkorn, F. E. (2019). High-speed X-ray investigation of melt dynamics during continuous-wave laser remelting of selective laser melted Co-Cr alloy. *CIRP Annals, 68*(1), 229–232. https://doi.org/10.1016/j.cirp.2019.04.110

Rieder, H., Spies, M., Bamberg, J., & Henkel, B. (2016). On- and offline ultrasonic characterization of components built by SLM additive manufacturing. In *AIP conference proceedings.*

Salarian, M., Asgari, H., & Vlasea, M. (2020). Pore space characteristics and corresponding effect on tensile properties of Inconel 625 fabricated via laser powder bed fusion. *Materials Science and Engineering A, 769*, 138525. https://doi.org/10.1016/j.msea.2019.138525

Sammons, P. M., Gegel, M. L., Bristow, D. A., & Landers, R. G. (2019). Repetitive process control of additive manufacturing with application to laser metal deposition. *IEEE Transactions on Control Systems Technology, 27*(2), 566–575. https://doi.org/10.1109/TCST.2017.2781653

Scime, L., & Beuth, J. (2018a). Anomaly detection and classification in a laser powder bed additive manufacturing process using a trained computer vision algorithm. *Additive Manufacturing, 19*, 114–126. https://doi.org/10.1016/j.addma.2017.11.009

Scime, L., & Beuth, J. (2018b). A multi-scale convolutional neural network for autonomous anomaly detection and classification in a laser powder bed fusion additive manufacturing process. *Additive Manufacturing, 24*, 273–286. https://doi.org/10.1016/j.addma.2018.09.034

Scime, L., & Beuth, J. (2019). Using machine learning to identify in-situ melt pool signatures indicative of flaw formation in a laser powder bed fusion additive manufacturing process. *Additive Manufacturing, 25*, 151–165. https://doi.org/10.1016/j.addma.2018.11.010

Scime, L., Siddel, D., Baird, S., & Paquit, V. (2020). Layer-wise anomaly detection and classification for powder bed additive manufacturing processes: A machine-agnostic algorithm for real-time pixel-wise semantic segmentation. *Additive Manufacturing, 36*, 101453. https://doi.org/10.1016/j.addma.2020.101453

Shaunak, S., Dhinsa, B. S., & Khan, W. S. (2017). The role of 3D modelling and printing in orthopaedic tissue engineering: A review of the current literature. *Current Stem Cell Research and Therapy, 12*(3), 225–232. https://doi.org/10.2174/1574888X11666160429122238

Shevchik, S. A., Kenel, C., Leinenbach, C., & Wasmer, K. (2018). Acoustic emission for in situ quality monitoring in additive manufacturing using spectral convolutional neural networks. *Additive Manufacturing, 21*, 598–604. https://doi.org/10.1016/j.addma.2017.11.012

Shevchik, S. A., Masinelli, G., Kenel, C., Leinenbach, C., & Wasmer, K. (2019). Deep learning for in situ and real-time quality monitoring in additive manufacturing using acoustic emission. *IEEE Transactions on Industrial Informatics, 15*(9), 5194–5203. https://doi.org/10.1109/TII.2019.2910524

Shin, J., & Mazumder, J. (2018). Composition monitoring using plasma diagnostics during direct metal deposition (DMD) process. *Optics and Laser Technology, 106*, 40–46. https://doi.org/10.1016/j.optlastec.2018.03.020

Silbernagel, C., Aremu, A., & Ashcroft, I. (2019). Using machine learning to aid in the parameter optimisation process for metal-based additive manufacturing. *Rapid Prototyping Journal, 26*(4), 625–637. https://doi.org/10.1108/RPJ-08-2019-0213

Smith, R. J., Hirsch, M., Patel, R., Li, W., Clare, A. T., & Sharples, S. D. (2016). Spatially resolved acoustic spectroscopy for selective laser melting. *Journal of Materials Processing Technology, 236*, 93–102. https://doi.org/10.1016/j.jmatprotec.2016.05.005

Snow, Z., Diehl, B., Reutzel, E. W., & Nassar, A. (2021). Toward in-situ flaw detection in laser powder bed fusion additive manufacturing through layerwise imagery and machine learning. *Journal of Manufacturing Systems, 59*, 12–26. https://doi.org/10.1016/j.jmsy.2021.01.008

Song, L., Huang, W., Han, X., & Mazumder, J. (2017). Real-time composition monitoring using support vector regression of laser-induced plasma for laser additive manufacturing. *IEEE Transactions on Industrial Electronics, 64*(1), 633–642. https://doi.org/10.1109/TIE.2016.2608318

Soni, B., Mathur, P., & Bora, A. (2021). In depth analysis, applications and future issues of artificial neural network. In A.-E. Hassanien, M. H. N. Taha, & N. E. M. Khalifa (Eds.), *Enabling AI applications in data science* (pp. 149–183). Springer. https://doi.org/10.1007/978-3-030-52067-0_7

Spears, T. G., & Gold, S. A. (2016). In-process sensing in selective laser melting (SLM) additive manufacturing. *Integrating Materials and Manufacturing Innovation, 5*(1), 16–40. https://doi.org/10.1186/s40192-016-0045-4

Spurek, M. A., Spierings, A. B., Lany, M., Revaz, B., Santi, G., Wicht, J., & Wegener, K. (2022). In-situ monitoring of powder bed fusion of metals using eddy current testing. *Additive Manufacturing, 60*, 103259. https://doi.org/10.1016/j.addma.2022.103259

Stockman, T., Horan, C., Knapp, C., Henderson, K., Patterson, B., Carpenter, J., & Schneider, J. (2019). Differentiating defect types in LENS™ metal AM via in situ pyrometer process monitoring. In *Minerals, metals and materials series* (pp. 197–204).

Sun, S., Brandt, M., & Easton, M. (2017). 2 - Powder bed fusion processes: An overview. In M. Brandt (Ed.), *Laser additive manufacturing* (pp. 55–77). Woodhead Publishing. https://doi.org/10.1016/B978-0-08-100433-3.00002-6

Sutton, R. S., & Barto, A. G. (2018). *Reinforcement learning: An introduction*. MIT Press.

Tang, Z. J., Liu, W. W., Wang, Y. W., Saleheen, K. M., Liu, Z. C., Peng, S. T., Zhang, Z., & Zhang, H. C. (2020). A review on in situ monitoring technology for directed energy deposition of metals. *International Journal of Advanced Manufacturing Technology*. https://doi.org/10.1007/s00170-020-05569-3

Thompson, S. M., Bian, L., Shamsaei, N., & Yadollahi, A. (2015). An overview of direct laser deposition for additive manufacturing; Part I: Transport phenomena, modeling and diagnostics. *Additive Manufacturing, 8*, 36–62. https://doi.org/10.1016/j.addma.2015.07.001

Toyserkani, E., Sarker, D., Ibhadode, O. O., Liravi, F., Russo, P., & Taherkhani, K. (2021). *Metal additive manufacturing*. Wiley. https://doi.org/10.1002/9781119210801

Valdiande, J., Mirapeix, J., Nin, J., Font, E., Seijas, C., & Higuera, J. M. L. (2021). Laser metal deposition on-line monitoring via plasma emission spectroscopy and spectral correlation techniques. *IEEE Journal of Selected Topics in Quantum Electronics*. https://doi.org/10.1109/JSTQE.2021.3075489

Wang, S., Wang, Y., Liu, C., & Mazumder, J. (2020). In-situ monitoring on micro-hardness of laser molten zone on AISI4140 steel by spectral analysis. *Scientific Reports, 10*(1), 4241. https://doi.org/10.1038/s41598-019-55559-z

Wang, W., Ning, J., & Liang, S. Y. (2021). In-situ distortion prediction in metal additive manufacturing considering boundary conditions. *International Journal of Precision Engineering and Manufacturing*. https://doi.org/10.1007/s12541-021-00496-z

Wasmer, K., Kenel, C., Leinenbach, C., & Shevchik, S. A. (2018a). In situ and real-time monitoring of powder-bed AM by combining acoustic emission and artificial intelligence. In M. Meboldt

& C. Klahn (Eds.), *Industrializing additive manufacturing—Proceedings of additive manufacturing in products and applications—AMPA2017*.

Wasmer, K., Le-Quang, T., Meylan, B., & Shevchik, S. A. (2019). In situ quality monitoring in AM using acoustic emission: A reinforcement learning approach. *Journal of Materials Engineering and Performance, 28*(2), 666–672. https://doi.org/10.1007/s11665-018-3690-2

Wasmer, K., Le-Quang, T., Meylan, B., Vakili-Farahani, F., Olbinado, M., Rack, A., & Shevchik, S. (2018b). Laser processing quality monitoring by combining acoustic emission and machine learning: A high-speed X-ray imaging approach. *Procedia CIRP, 74*, 654–658.

Westphal, E., & Seitz, H. (2021). A machine learning method for defect detection and visualization in selective laser sintering based on convolutional neural networks. *Additive Manufacturing, 41*, 101965. https://doi.org/10.1016/j.addma.2021.101965

Williams, J., Dryburgh, P., Clare, A., Rao, P., & Samal, A. (2018). Defect detection and monitoring in metal additive manufactured parts through deep learning of spatially resolved acoustic spectroscopy signals. *Smart and Sustainable Manufacturing Systems, 2*(1), 20180035.

Withers, P. J., Bouman, C., Carmignato, S., Cnudde, V., Grimaldi, D., Hagen, C. K., Maire, E., Manley, M., Du Plessis, A., & Stock, S. R. (2021). X-ray computed tomography. *Nature Reviews Methods Primers, 1*(1), 18. https://doi.org/10.1038/s43586-021-00015-4

Wohlers, T., & Gornet, T. (2014). History of additive manufacturing. *Wohlers Report, 24*(2014), 118.

Wu, B., Ji, X. Y., Zhou, J. X., Yang, H. Q., Peng, D. J., Wang, Z. M., Wu, Y. J., & Yin, Y. J. (2021). In situ monitoring methods for selective laser melting additive manufacturing process based on images—A review. *China Foundry, 18*(4), 265–285. https://doi.org/10.1007/s41230-021-1111-x

Wu, Z., Rincon, D., & Christofides, P. D. (2020). Real-time adaptive machine-learning-based predictive control of nonlinear processes. *Industrial and Engineering Chemistry Research, 59*(6), 2275–2290. https://doi.org/10.1021/acs.iecr.9b03055

Xiao, X., Liu, X., Cheng, M., & Song, L. (2020). Towards monitoring laser welding process via a coaxial pyrometer. *Journal of Materials Processing Technology, 277*, 116409. https://doi.org/10.1016/j.jmatprotec.2019.116409

Xiong, J., Liu, G., & Pi, Y. (2019). Increasing stability in robotic GTA-based additive manufacturing through optical measurement and feedback control. *Robotics and Computer-Integrated Manufacturing, 59*, 385–393. https://doi.org/10.1016/j.rcim.2019.05.012

Ya, W., Konuk, A. R., Aarts, R., Pathiraj, B., & Huis in't Veld, B. (2015). Spectroscopic monitoring of metallic bonding in laser metal deposition. *Journal of Materials Processing Technology, 220*, 276–284. https://doi.org/10.1016/j.jmatprotec.2015.01.026

Yadav, P., Singh, V. K., Joffre, T., Rigo, O., Arvieu, C., Le Guen, E., & Lacoste, E. (2020). Inline drift detection using monitoring systems and machine learning in selective laser melting. *Advanced Engineering Materials*. https://doi.org/10.1002/adem.202000660

Yadroitsev, I., Yadroitsava, I., Du Plessis, A., & MacDonald, E. (2021). *Fundamentals of laser powder bed fusion of metals* (Additive Manufacturing Materials and Technologies ed.). S.l. : ELSEVIER.

Yang, L., Lo, L., Ding, S., & Özel, T. (2020). Monitoring and detection of meltpool and spatter regions in laser powder bed fusion of super alloy Inconel 625. *Progress in Additive Manufacturing*. https://doi.org/10.1007/s40964-020-00140-8

Ye, D., His Fuh, J. Y., Zhang, Y., Hong, G. S., & Zhu, K. (2018b). In situ monitoring of selective laser melting using plume and spatter signatures by deep belief networks. *ISA Transactions, 81*, 96–104. https://doi.org/10.1016/j.isatra.2018.07.021

Ye, D., Hong, G. S., Zhang, Y., Zhu, K., & Fuh, J. Y. H. (2018a). Defect detection in selective laser melting technology by acoustic signals with deep belief networks. *International Journal of Advanced Manufacturing Technology, 96*(5–8), 2791–2801. https://doi.org/10.1007/s00170-018-1728-0

Ye, J., Bab-Hadiashar, A., Hoseinnezhad, R., Alam, N., Vargas-Uscategui, A., Patel, M., & Cole, I. (2022). Predictions of in-situ melt pool geometric signatures via machine learning techniques for laser metal deposition. *International Journal of Computer Integrated Manufacturing*. https://doi.org/10.1080/0951192X.2022.2048422

Yeung, H., Yang, Z., & Yan, L. (2020). A meltpool prediction based scan strategy for powder bed fusion additive manufacturing. *Additive Manufacturing, 35*, 101383. https://doi.org/10.1016/j.addma.2020.101383

Yuan, B., Giera, B., Guss, G., Matthews, I., & Mcmains, S. (2019, 7–11 Jan. 2019). Semi-supervised convolutional neural networks for in-situ video monitoring of selective laser melting. In *2019 IEEE winter conference on applications of computer vision* (*WACV*).

Yuan, B., Guss, G. M., Wilson, A. C., Hau-Riege, S. P., DePond, P. J., McMains, S., Matthews, M. J., & Giera, B. (2018). Machine-learning-based monitoring of laser powder bed fusion. *Advanced Materials Technologies, 3*(12), 1800136. https://doi.org/10.1002/admt.201800136

Zavalov, Y. N., Dubrov, A. V., & Dubrov, V. D. (2019). Optical method of on-line temperature monitoring on the melt surface in laser metal deposition technology. *Proceedings of SPIE* - The International Society for Optical Engineering,

Zhang, B., Jaiswal, P., Rai, R., Guerrier, P., & Baggs, G. (2019a). Convolutional neural network-based inspection of metal additive manufacturing parts. *Rapid Prototyping Journal, 25*(3), 530–540. https://doi.org/10.1108/RPJ-04-2018-0096

Zhang, X., Chueh, Y. H., Wei, C., Sun, Z., Yan, J., & Li, L. (2020). Additive manufacturing of three-dimensional metal-glass functionally gradient material components by laser powder bed fusion with in situ powder mixing. *Additive Manufacturing, 33*, 101113. https://doi.org/10.1016/j.addma.2020.101113

Zhang, Y., Hong, G. S., Ye, D., Zhu, K., & Fuh, J. Y. H. (2018). Extraction and evaluation of melt pool, plume and spatter information for powder-bed fusion AM process monitoring. *Materials & Design, 156*, 458–469. https://doi.org/10.1016/j.matdes.2018.07.002

Zhang, Z., Wu, X., & Tan, J. (2019b). In-situ monitoring of stress corrosion cracking of 304 stainless steel in high-temperature water by analyzing acoustic emission waveform. *Corrosion Science, 146*, 90–98. https://doi.org/10.1016/j.corsci.2018.10.022

Zhao, C., Fezzaa, K., Cunningham, R. W., Wen, H., De Carlo, F., Chen, L., Rollett, A. D., & Sun, T. (2017). Real-time monitoring of laser powder bed fusion process using high-speed X-ray imaging and diffraction. *Scientific Reports, 7*(1), 3602. https://doi.org/10.1038/s41598-017-03761-2

Zhiyuan Xu, A., Bo Chen, B., Caiwang Tan, C., & Jicai Feng, D. (2019). Inconel625/316L functionally graded material using spectral diagnostics during laser additive manufacturing process. *Journal of Laser Applications, 31*(2), 022001. https://doi.org/10.2351/1.5070116

Zhu, B., & Xiong, J. (2020). Increasing deposition height stability in robotic GTA additive manufacturing based on arc voltage sensing and control. *Robotics and Computer-Integrated Manufacturing, 65*, 101977. https://doi.org/10.1016/j.rcim.2020.101977

Publisher's Note Springer Nature remains neutral with regard to jurisdictional claims in published maps and institutional affiliations.